

- [70] R. Edelman, K. Palmer, K. G. Russ et al., "Safety and immunogenicity of recombinant Bacille Calmette-Guerin (rBCG) expressing *Borrelia burgdorferi* outer surface protein A (OspA) lipoprotein in adult volunteers: a candidate Lyme disease vaccine," *Vaccine*, vol. 17, no. 7-8, pp. 904–914, 1999.
- [71] S. Matsumoto, H. Yukitake, H. Kanbara, and T. Yamada, "Recombinant *Mycobacterium bovis* bacillus Calmette-Guerin secreting merozoite surface protein 1 (MSP1) induces protection against rodent malaria parasite infection depending on MSP1-stimulated interferon γ and parasite-specific antibodies," *Journal of Experimental Medicine*, vol. 188, no. 5, pp. 845–854, 1998.
- [72] C. Zheng, P. Xie, and Y. Chen, "Recombinant *Mycobacterium bovis* BCG producing the circumsporozoite protein of *Plasmodium falciparum* FCC-1/HN strain induces strong immune responses in BALB/c mice," *Parasitology International*, vol. 51, no. 1, pp. 1–7, 2002.
- [73] Y. D. Zhu, G. Fennelly, C. Miller et al., "Recombinant bacille Calmette-Guérin expressing the measles virus nucleoprotein protects infant rhesus macaques from measles virus pneumonia," *Journal of Infectious Diseases*, vol. 176, no. 6, pp. 1445–1453, 1997.
- [74] S. Uno-Furuta, K. Matsuo, S. Tamaki et al., "Immunization with recombinant Calmette-Guerin bacillus (BCG)-hepatitis C virus (HCV) elicits HCV-specific cytotoxic T lymphocytes in mice," *Vaccine*, vol. 21, no. 23, pp. 3149–3156, 2003.

In Vivo Safety and Persistence of Endoribonuclease Gene-Transduced CD4+ T Cells in Cynomolgus Macaques for HIV-1 Gene Therapy Model

Hideto Chono^{1*}, Naoki Saito¹, Hiroshi Tsuda¹, Hiroaki Shibata², Naohide Ageyama², Keiji Terao², Yasuhiro Yasutomi², Junichi Mineno¹, Ikunoshin Kato¹

¹ Center for Cell and Gene Therapy, Takara Bio Inc, Otsu, Shiga, Japan, ² Tsukuba Primate Research Center, National Institute of Biomedical Innovation, Tsukuba, Ibaraki, Japan

Abstract

Background: MazF is an endoribonuclease encoded by *Escherichia coli* that specifically cleaves the ACA sequence of mRNA. In our previous report, conditional expression of MazF in the HIV-1 LTR rendered CD4+ T lymphocytes resistant to HIV-1 replication. In this study, we examined the *in vivo* safety and persistence of MazF-transduced cynomolgus macaque CD4+ T cells infused into autologous monkeys.

Methodology/Principal Findings: The *in vivo* persistence of the gene-modified CD4+ T cells in the peripheral blood was monitored for more than half a year using quantitative real-time PCR and flow cytometry, followed by experimental autopsy in order to examine the safety and distribution pattern of the infused cells in several organs. Although the levels of the MazF-transduced CD4+ T cells gradually decreased in the peripheral blood, they were clearly detected throughout the experimental period. Moreover, the infused cells were detected in the distal lymphoid tissues, such as several lymph nodes and the spleen. Histopathological analyses of tissues revealed that there were no lesions related to the infused gene modified cells. Antibodies against MazF were not detected. These data suggest the safety and the low immunogenicity of MazF-transduced CD4+ T cells. Finally, gene modified cells harvested from the monkey more than half a year post-infusion suppressed the replication of SHIV 89.6P.

Conclusions/Significance: The long-term persistence, safety and continuous HIV replication resistance of the *mazF* gene-modified CD4+ T cells in the non-human primate model suggests that autologous transplantation of *mazF* gene-modified cells is an attractive strategy for HIV gene therapy.

Citation: Chono H, Saito N, Tsuda H, Shibata H, Ageyama N, et al. (2011) *In Vivo* Safety and Persistence of Endoribonuclease Gene-Transduced CD4+ T Cells in Cynomolgus Macaques for HIV-1 Gene Therapy Model. PLoS ONE 6(8): e23585. doi:10.1371/journal.pone.0023585

Editor: John J. Rossi, Beckman Research Institute of the City of Hope, United States of America

Received: January 10, 2011; **Accepted:** July 20, 2011; **Published:** August 17, 2011

Copyright: © 2011 Chono et al. This is an open-access article distributed under the terms of the Creative Commons Attribution License, which permits unrestricted use, distribution, and reproduction in any medium, provided the original author and source are credited.

Funding: The authors have no support or funding to report.

Competing Interests: Hideto Chono, Naoki Saito, Hiroshi Tsuda, Junichi Mineno and Ikunoshin Kato are employees of Takara Bio Inc. (<http://www.takara-bio.co.jp>). There are no patents, products in development or marketed products to declare. This does not alter the authors' adherence to all the PLoS ONE policies on sharing data and materials.

* E-mail: chonoh@takara-bio.co.jp

Introduction

Highly active anti-retroviral therapy (HAART) is widely used for human immunodeficiency virus (HIV) therapy and involves the combination of several drugs with different functions that are currently being evaluated in clinical trials; some of these drugs are currently available [1]. HAART treatment reduces plasma viral load to undetectable levels and recovers CD4+ T cells to clinically safe levels. Although HAART therapy has revolutionized the treatment of HIV-1 infection, the need for life-long therapy, difficulties with medication adherence and long-term medication toxicities have led to the search for new treatment strategies that will efficiently reduce the viral load and allow for stable immunological homeostasis. The number of patients who are HAART resistant has significantly decreased in the past 2 years due to newly available drugs, but based on previous experience, drug resistance is likely to increase again. Thus, additional approaches for the management of HIV infection, or approaches

performed in combination with HAART therapy, are needed. Gene therapy for HIV-1 infection has been proposed as an alternative to antiretroviral drug regimens [2,3]. A number of different genetic vectors with antiviral payloads have been utilized to combat HIV-1, including antisense RNA against the HIV-1 envelope gene, transdominant protein RevM10, ribozymes, RNA decoys, single chain antibodies, and RNA-interference [4,5]. These protocols use T cells or hematopoietic stem cells as a target for gene modification. Autologous T cell transfer in HIV patients began in the mid 1990's, and since that time, no serious adverse events have been reported to be associated with infusions of autologous T cells, and infusions are well tolerated. The majority of these clinical trials used gene transfer by retrovirus or lentiviral vectors for the delivery of the anti-HIV payloads.

In order to develop a new approach for HIV therapy, we previously constructed an HIV-1 Tat-dependent expression retroviral vector in which the *Escherichia coli* (*E. coli*) endoribonuclease gene *mazF* was fused downstream of the trans-activation

response element (TAR) so that the gene expression of *mazF* is induced upon HIV-1 replication [6]. When MazF-transduced cells were infected with HIV-1 IIB, the replication of HIV-1 was efficiently inhibited without affecting CD4+ T cell growth. MazF-transduced primary CD4+ T cells derived from monkeys also suppressed simian/human immunodeficiency virus (SHIV) replication [6]. Thus, autologous transfer of genetically modified CD4+ T cells conditionally expressing the MazF protein will be a promising strategy for HIV gene therapy. Generally, the shift from the chronic phase to the AIDS phase is due to the balance between viral growth and immune suppression, and the remarkable decrease in CD4+ T cells causes the subsequent deficiency of the immune system, the hallmarks of AIDS. The benefit of the MazF-based gene therapy strategy is that gene-modified CD4+ T cells may be protected from HIV-1-associated cell death and are therefore likely to help the immune system maintain a stable condition.

In this preclinical study, we examined the *in vivo* safety and persistence of MazF-transduced autologous CD4+ T cells (named MazF-Tmac cells) using a non-human primate model. Cynomolgus macaque primary CD4+ T cells were retrovirally transduced with the MazF vector, infused into the autologous monkeys, and the persistence and safety of the MazF-Tmac cells was monitored more than half a year. We found that infused MazF-Tmac cells were detected in the peripheral blood throughout the experimental period. Additionally, experimental autopsy revealed the distribution of the infused lymphocyte in total body.

Results

Manufacturing of MazF-transduced CD4+ T cells using *ex vivo*-expanded cynomolgus macaque CD4+ T cells

In order to infuse more than 1×10^9 MazF-transduced autologous cells, isolated primary CD4+ T lymphocytes were *ex vivo* stimulated, transduced with the MT-MFR-PL2 retroviral vector (Figure 1A), and expanded as described in the Materials and Methods. The resultant MazF-Tmac cells were transplanted into autologous monkeys via intravenous infusion (Figure 1B). We initially used concanavalin A (Con A) for the stimulation of CD4+ T cells (CD4T-1), but Con A only induced a 12-fold cell expansion after 7 days. In order to improve the *ex vivo* expansion, we used anti-CD3/anti-CD28 monoclonal antibody-conjugated beads (anti-CD3/CD28 beads), which are known to yield a more efficient cellular expansion [7,8]. As we expected, the fold expansion of CD4+ T cells (CD4T-2 and CD4T-3) stimulated with anti-CD3/CD28 beads was much higher than with Con A stimulation (Table 1). In order to improve the engraftment efficiency of CD4+ T cells, busulfan was orally administered to the macaques prior to the transplantation, and the gene-modified MazF-Tmac cells were infused into each monkey intravenously at $1.6\text{--}2.7 \times 10^9$ cells.

Transduction efficiency and cell surface markers of MazF-Tmac cells

The efficiency of MazF transduction and phenotype of cell surface markers of the MazF-Tmac cells were analyzed using flow cytometry. The MazF vector transduction efficiency of CD4T-2 and CD4T-3 cells was 61.8% and 60.0%, respectively, while only 34.5% for CD4T-1 (Table 1). As shown in Table 2, 99% of the expanded MazF-Tmac cells were CD3 and CD4 double-positive, and in these cells, more than 90% expressed CD95/CD28, which are known central memory phenotype markers [9]. Central memory cells generally have a longer life span compared to effector memory cells [10]; thus, a higher percentage of central

memory cells in MazF-Tmac cells is likely to result in longer persistence after transplantation. Furthermore, to assess the activation status of MazF-Tmac cells, we measured the expression of CD25, which is also known as IL-2 receptor alpha and is an activated T cell marker. CD25 expression of MazF-Tmac cells from CD4T-2 and CD4T-3 was low. In contrast, almost 100% of the CD4+ T cells were found to express CD25 with a higher expression level 2–4 days after stimulation (data not shown). Thus, these data indicate that a large number of MazF-Tmac cells entered into resting or non-activated states during the *ex vivo* culture. CXCR4, a co-receptor for X4 tropic HIV entry, was found to be expressed in expanded CD4T-2 and CD4T-3 MazF-Tmac cells. Furthermore, we observed that there was no significant difference in the measured cell surface markers between Con A- and anti-CD3/CD28 bead-stimulated MazF-Tmac cells (Table 2).

Longitudinal analysis of infused MazF-Tmac cells

To examine the *in vivo* safety and persistence of infused MazF-Tmac cells, peripheral blood from each monkey was collected to monitor the hematological effects and the proviral copy number of the transduced retroviral vector in the genome over six months. There was no significant change in the body weight of the monkeys throughout the experiment (Figure 2A). During the period of 2–4 weeks post-transplantation, severe reduction in the white blood cell (WBC) count, hemoglobin (Hb) concentration, and platelet (PLT) levels were observed in the monkeys CD4T-1 and CD4T-2, while only slight reduction was observed in CD4T-3. These negative effects are considered to be due to the effect of the busulfan treatment, which is known to cause partial bone marrow depletion and functional defects in blood-forming tissues. No other adverse events were observed throughout the experiments. The transient reduction of lymphocytes gradually recovered, and the cell number became stable two months after the transplantation (Figure 2A).

The percentage of persistent MazF-Tmac cells in CD4+ T cells was determined using real-time PCR and flow cytometric analyses. The percentage of MazF-Tmac cells gradually decreased in CD4T-1- and CD4T-2-transplanted monkeys, while in the CD4T-3-transplanted monkey, a drastic reduction of the infused MazF-Tmac cells was observed 3–4 weeks post-transplantation but was not observed at later time points (Figure 2B). Although the levels of MazF-Tmac cells gradually decreased over time, the infused MazF-Tmac cells were detected even after six months post-transplantation. It is reasonable to assume that a population of infused MazF-Tmac cells can persist for a long-term period, likely forming a resting condition.

Detection of anti-MazF antibodies in monkey blood

Although the levels of MazF-transduced CD4+ T cells gradually decreased in the peripheral blood, some were detected throughout the half-year experimental period, suggesting that MazF-Tmac cells showed little or no immunogenicity towards cynomolgus macaques. Because gene therapy for HIV is aimed at reconstituting an HIV-resistant immune system, genetically modified cells must not only inhibit virus replication, but also maintain their expected trafficking behavior and persist *in vivo*. Although the evidence of longitudinal persistence of MazF-Tmac cells supports the low immunogenicity of MazF-Tmac cells, it is important to assess the production of antibodies against MazF. As shown in Figure 3 and Figure S1, we detected no production of anti-MazF antibodies in the CD4T-2 monkey blood after transplantation of the MazF-Tmac cells.

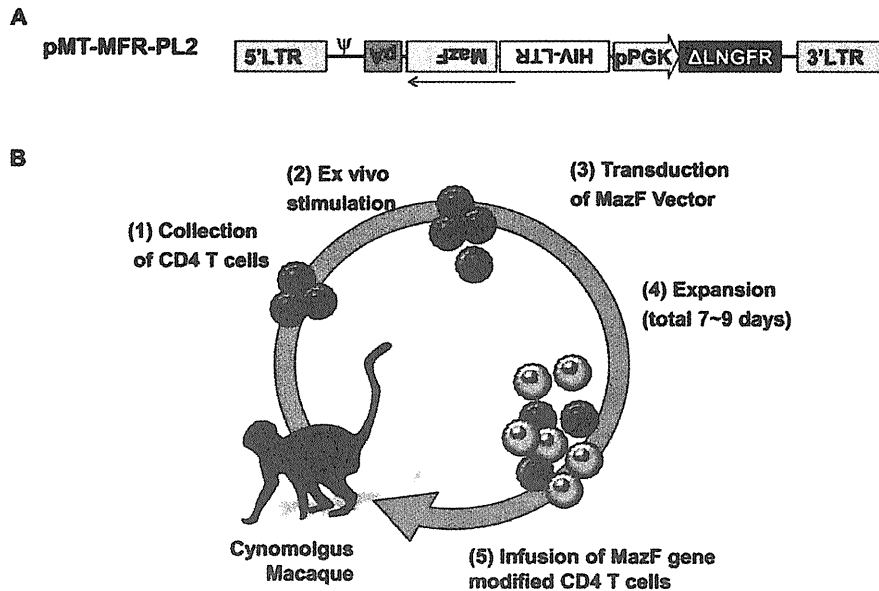


Figure 1. Diagram of autologous CD4+ T cell transplantation using a non-human primate model. (A) Design of gene transfer vector. The MazF gene derived from *E. coli* was inserted directly into the downstream of HIV-LTR sequence. The HIV-LTR-MazF-polyA cassette was introduced in the opposite direction of the MoMLV-LTR. A truncated form of the human Δ LINGFR was also introduced into the retrovirus vector as a surface marker. The Δ LINGFR gene is under the control of the human PGK promoter. (B) Flow diagram of gene-transduced CD4+ T cell manufacture. (1) Peripheral blood was collected by apheresis, (2) CD4+ T cells were selected by positive selection and stimulated *ex vivo* with Con A or anti-CD3/CD28 monoclonal antibody-conjugated beads. (3) The MT-MFR-PL2 vector was transduced twice on days 3 and 4. (4) The transduced cells were expanded for an additional 3–5 days until the total cell number reached more than 10^9 . (5) On day 7–9, the expanded cells were collected, washed, and infused to the autologous macaques through venous blood. doi:10.1371/journal.pone.0023585.g001

In vivo safety of MazF-Tmac cells

It is a great advantage to use primate models for investigating the safety of gene-modified cells, as they can be used for surgical pathological analysis. Therefore, we performed experimental autopsies six months after transplantation. To examine the safety of MazF-Tmac cells, specimens from several organs were fixed in buffered formaldehyde and embedded in plastic. Serial sections were made using a diamond saw. Slides were then stained with hematoxylin-eosin. Histopathological findings of the specimens were contracted with Bozo Research Center (Tokyo, Japan), and no severe adverse events relating to MazF-Tmac cell infusion was observed (Table 3 and Figure S2).

Table 1. Demographic data and summary of expansion fold and transduction efficiency.

| | CD4T-1 | CD4T-2 | CD4T-3 |
|--|--------|---------------------|---------------------|
| Body Weight (kg) | 5.25 | 5.18 | 3.7 |
| Method for stimulation | Con A | Anti-CD3/CD28 Beads | Anti-CD3/CD28 Beads |
| Number of stimulated CD4+ T cells ($\times 10^7$ cells) | 13.0 | 1.0 | 4.6 |
| Days for expansion (days) | 7 | 7 | 9 |
| Number of infused MazF-Tmac cells ($\times 10^9$ cells) | 1.6 | 1.7 | 2.7 |
| Expansion Fold | 12.3 | 170 | 58.7 |
| Gene transfer efficiency (%) | 34.5 | 61.8 | 60.0 |

doi:10.1371/journal.pone.0023585.t001

Examination of the anti-viral efficacy of MazF-Tmac cells harvested from monkey

In order to examine whether the Tat-dependent expression of MazF and anti-viral efficacy was maintained in the MazF-Tmac cells after infusion, CD4+ T lymphoid cells from a CD4T-1-transplanted monkey (214 days post-infusion of MazF-Tmac cells) were selected and expanded *ex vivo* (Figure 4A). After 7 days of expansion, the genetically modified cells expressing a truncated form of the human low affinity nerve growth factor (Δ LINGFR+) were concentrated with an anti-CD271 monoclonal antibody (Figure 4B). CD271-positive cells and CD271-negative cells were expanded for an additional 4 days. Both groups of expanded cells were infected with SHIV 89.6P [11] at the multiplicity of infection (MOI) of 0.01. Culture supernatants and cell pellets were analyzed at 6 days post-infection. As shown in Figure 4C, the replication of SHIV 89.6P was significantly suppressed in CD271-positive cells

Table 2. Cell surface markers of expanded MazF-Tmac cells.

| | CD4T-1 | CD4T-2 | CD4T-3 |
|-----------------------------|--------|--------|--------|
| CD3(+)/CD4(+) (%) | 98.2 | 98.7 | 99.9 |
| CD95(-)/CD28(+) (Naïve) (%) | 0.7 | 1.2 | 0.4 |
| CD95(+)/CD28(+) (CM) (%) | 93.0 | 94.7 | 91.2 |
| CD95(+)/CD28(-) (EM) (%) | 6.2 | 3.9 | 8.3 |
| CXCR4 (%) | N/A | 92.0 | 79.4 |
| CD25 (%) | N/A | 30.4 | 24.5 |

CM: Central Memory, EM: Effector Memory.
doi:10.1371/journal.pone.0023585.t002

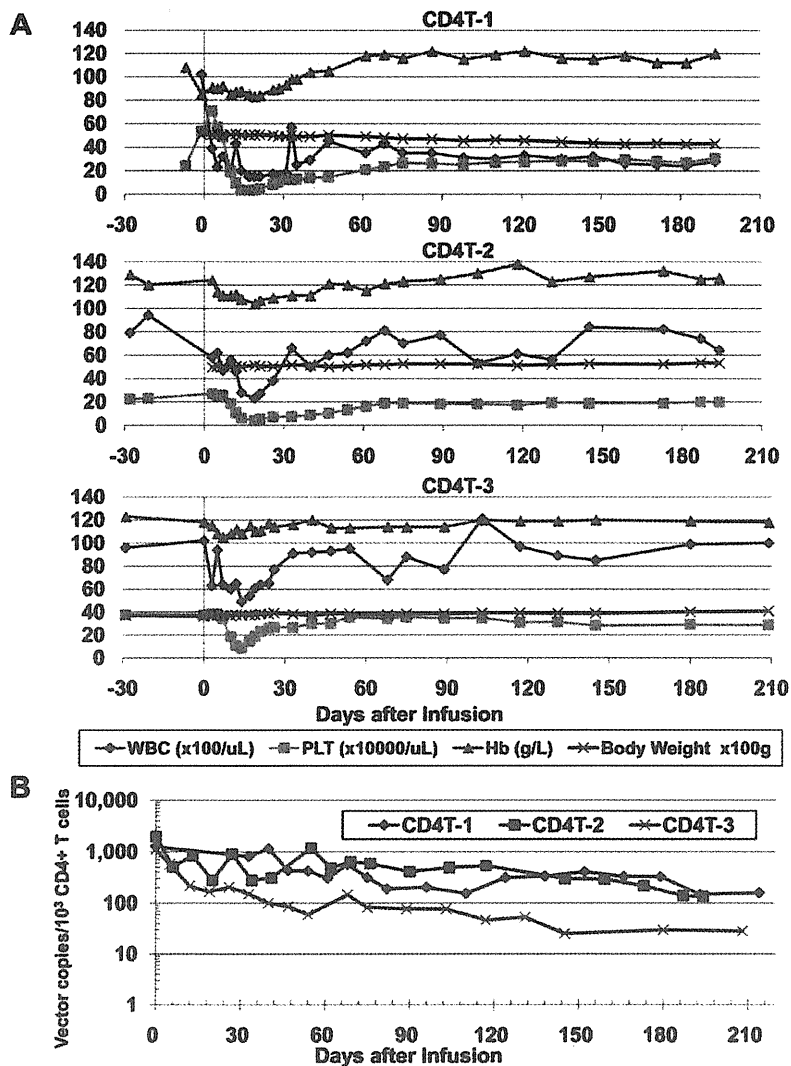


Figure 2. Hematological analysis and engraftment of the MazF-transduced CD4+ T cells. (A) The body weight and several hematological features were measured at the indicated time points, and the number of WBC, Hb, and PLT were represented. Each macaque was monitored throughout the study period. (B) The *in vivo* persistence of retroviral-transduced CD4+ T cells in the peripheral blood. PBMCs were collected at the indicated time points. The percentage of CD4+ T cells was analyzed using flow cytometry, and the proviral MazF vector copy was analyzed using real-time PCR. By compounding these two data, the copy number of the *mazF* gene in CD4+ T cells was calculated. doi:10.1371/journal.pone.0023585.g002

in comparison with CD271-negative cells. Although western blot analysis managed to detect the expression of MazF, MazF was below the detection limit (data not shown). However, the expression of MazF was clearly induced when the same CD271-positive cells were transduced with the Tat expression retroviral vector M-LTR-Tat-ZG [6] (Figure 4D). These data suggest that the conditional expression system in MazF-Tmac cells is still active at 6 months post-transplantation.

Distribution of MazF-Tmac cells

To examine the distribution and persistence of the infused MazF-Tmac cells in a monkey, lymphocytes isolated from several organs were analyzed using flow cytometry and real-time PCR. As shown in Figure 5A and 5B, Δ LNFR+ cells were detected in CD4+ T cells isolated from several lymph nodes (LNs), spleen, and

peripheral blood. A similar tendency was obtained using real-time PCR (Figure 5C). In contrast, MazF-Tmac cells were not detected in the bone marrow, liver, thymus, and small intestine (data not shown). These data strongly suggest that infused MazF-Tmac cells mainly circulate in the secondary lymphoid organs.

In vivo distribution of MazF-Tmac cells treated with or without retinoic acid

Based on the findings that MazF-Tmac cells were well distributed among secondary lymphoid organs but not in small intestine, we performed additional experiment using one cynomolgus monkey (CD4T-4). In order to investigate the editing effect of the homing receptor to efficiently recruit the gene-modified cells to intestinal tissues in a non-human primate model, the distribution of retinoic acid-treated MazF-Tmac cells was

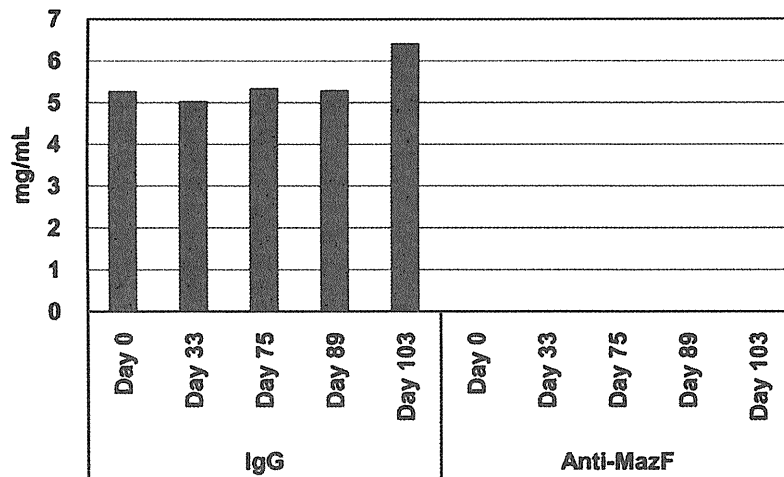


Figure 3. No detection of anti-MazF antibodies in monkey blood after transplantation of MazF-Tmac cells. Plasma samples were isolated from the monkey CD4T-2 at day 0, 33, 75, and 103 after transplantation and were used to detect anti-MazF antibodies on a MazF protein-immobilized microplate. The plasma samples were diluted to 500,000-fold, 50,000-fold, and 10,000-fold and added to each well. After the incubation, antibodies which reacted with immobilized MazF were tried to detect as described in Materials and Methods. No MazF-specific antibodies were detected.

doi:10.1371/journal.pone.0023585.g003

examined in a cynomolgus macaque. The experimental procedure is described in Figure 6A. Non-treated and retinoic acid-treated MazF-Tmac cells were designated as MazF-Tmac-N and MazF-Tmac-R, respectively. Expressions of integrin- $\alpha 4$ and integrin- $\beta 7$ were remarkably increased in the presence of retinoic acid (Figure 6B). Thereafter, MazF-Tmac-N and MazF-Tmac-R were labeled with carboxyfluorescein diacetate succinimidyl ester (CFSE) and PKH26, respectively. The CFSE-labeled cells were mixed with an equal number of PKH26-labeled cells (Figure 6C), and 6.8×10^8 of the mixed cells were infused into a CD4T-4 monkey. Note that the transduction efficiency of the MazF vector was 65% (data not shown). Three days after the transplantation, experimental autopsy was performed to obtain samples of several

organs as described in the Materials and Methods. Both the CFSE- and the PKH26-labeled CD4+ T cells were detected in the peripheral blood and several LNs by FACS analysis (Figure 6D). The percentage of the infused cells in the LNs was low compared to the peripheral blood, indicating that a large number of the infused cells did not migrate to the secondary lymphoid tissues and circulated in the peripheral blood at this time point. In the case of the inguinal and axillary LNs, the percentage of MazF-Tmac-R cells was low compared to MazF-Tmac-N cells. In contrast, a higher percentage of MazF-Tmac-R cells was observed in the mesenteric LN compared to MazF-Tmac-N cells. MazF-Tmac-N cells were evenly distributed in the three LNs analyzed, while the MazF-Tmac-R cells seemed to be preferentially distributed in the mesenteric LNs. Moreover, a large number of MazF-Tmac-R cells were distributed in the small intestine, while MazF-Tmac-N cells were not. To further evaluate the homing effect of the MazF-Tmac cells, the distribution of the labeled-MazF-Tmac cells in cryopreserved organs was analyzed using fluorescence microscopy (Figure 6E). A number of the PKH26-labeled MazF-Tmac-R cells were observed in the mesenteric LNs and in Peyer's patches. Taken together, retinoic acid-treated MazF-Tmac cells seem to be selectively recruited to mesenteric LNs and then transported to Peyer's patches. The distribution of MazF-Tmac-R cells in the intestinal villi remains to be determined.

Table 3. Analysis of *in vivo* safety (Histological finding about autopsy sample).

| | CD4T-1 | CD4T-2 | CD4T-3 |
|-----------------|--------|--------|--------|
| Lymph node | ± | ± | — |
| Spleen | — | — | ± |
| Bone marrow | ++** | — | — |
| Thymus | N/A | +* | — |
| Small intestine | — | — | — |
| Liver | — | — | — |
| Kidney | — | ± | — |
| Pancreas | — | — | — |
| Stomach | — | — | ± |
| Lung | — | ± | — |
| Heart | — | — | ± |

—: No remarkable changes; ±: Minimal; +: Mild; ++: Moderate.

N/A: No equivalent sample available.

*Due to the Aging,

**Side effect due to the busulfan administration.

doi:10.1371/journal.pone.0023585.t003

Discussion

MazF is a toxin encoded by the *E. coli* genome and plays a role in growth regulation under stress conditions in *E. coli* [12]. MazF can act as an endoribonuclease (RNase) that specifically cleaves cellular mRNAs at ACA sequences [13]. Therefore, MazF induction in *E. coli* virtually eliminates almost all cellular mRNAs to completely inhibit protein synthesis. However, MazF-induced cells retain full capacity for protein synthesis, as MazF-induced cells are able to produce a protein at a high level if the prerequisite mRNA is engineered to be devoid of all ACA sequences without altering its amino acid sequence [14]. This indicates that RNA components involved in protein synthesis are protected from

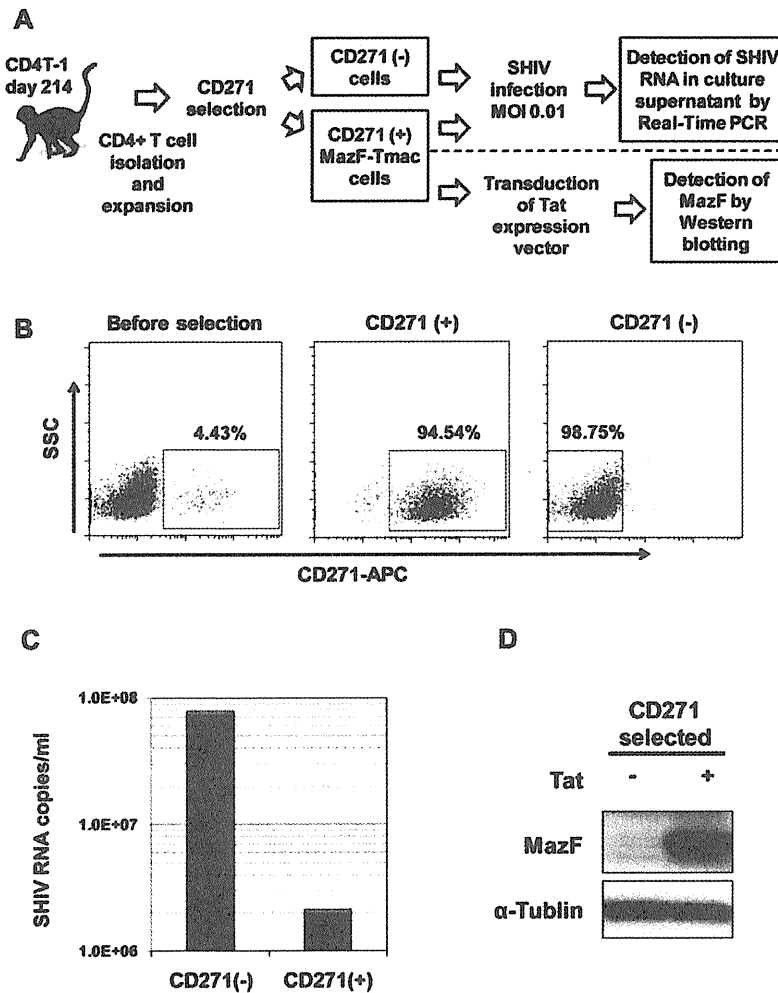


Figure 4. Examination of the anti-viral efficacy of MazF-Tmac cells harvested from the monkey. (A) Flow diagram of the experiment. CD4+ T lymphoid cells from CD4T-1 (214 days post-infusion of the MazF-Tmac cells) were stimulated and expanded *ex vivo*. The genetically modified cells expressing Δ LNFR+ were concentrated with an anti-CD271 monoclonal antibody and expanded for 4 days. The expanded CD271-enriched cells and CD271-negative cells were infected with SHIV 89.6P. SHIV RNA levels in the culture supernatant were determined using quantitative real-time PCR. Expression of MazF was detected from the cell lysates by western blot analysis. Moreover, CD271-positive cells were transduced with the Tat expression vector. (B) CD271-positive and -negative cells were enriched using an anti-CD271 antibody, and dot plots of the flow cytometry analysis are presented. (C) The suppression of SHIV RNA in the culture supernatant at 6 days after infection was detected by real-time PCR analysis. (D) MazF-Tmac cells transduced with the Tat expression vector were harvested at 20 hours post-transduction and used for western blot analysis. Conditional expression of MazF in a Tat-dependent manner was observed. doi:10.1371/journal.pone.0023585.g004

MazF cleavage. Indeed, ribosomal RNAs (rRNAs) and transfer RNAs (tRNAs) are protected from MazF cleavage in *E. coli* [15].

RNase-based anti-HIV gene therapy is an attractive strategy to suppress HIV-1 RNA replication. In the case of MazF, there are more than 240 ACA sequences in HIV-1 RNA, suggesting that HIV has almost no chance to gain MazF-related escape mutations. This approach seems to have a substantial advantage over the other known antiviral strategies, including antiviral drug therapy, and RNA-based gene therapies, such as antisense RNA, ribozyme, and siRNA.

MazF overexpressed in mammalian cells preferentially cleaves messenger RNAs (mRNAs), but not ribosomal RNAs [16]. As HIV-1 RNA has more than 240 ACA sequences, we assumed that the viral RNA is highly susceptible to MazF, leading to inhibition

of viral replication under a conditional expression system. Indeed, conditional expression of MazF with Tat suppresses replication of both HIV-1 IIB and SHIV 89.6P without affecting cellular mRNAs, suggesting that this Tat-dependent expression system of MazF is an attractive payload for HIV gene therapy [6]. It is an intriguing phenomenon that viral RNAs are efficiently and preferentially cleaved without affecting cellular mRNAs, and we are now addressing this question. Meanwhile, MazF is a bacterial protein, and its expression is induced by Tat protein; thus, it is important to assess the safety and immunogenicity of *mazF* gene-modified cells *in vivo*. In order to determine the safety of our MazF-retrovirus system *in vivo*, we infused MazF-transduced CD4+ T cells into cynomolgus macaques. In human gene therapy trials, engraftment of 1–2% of genetically modified cells in the peripheral

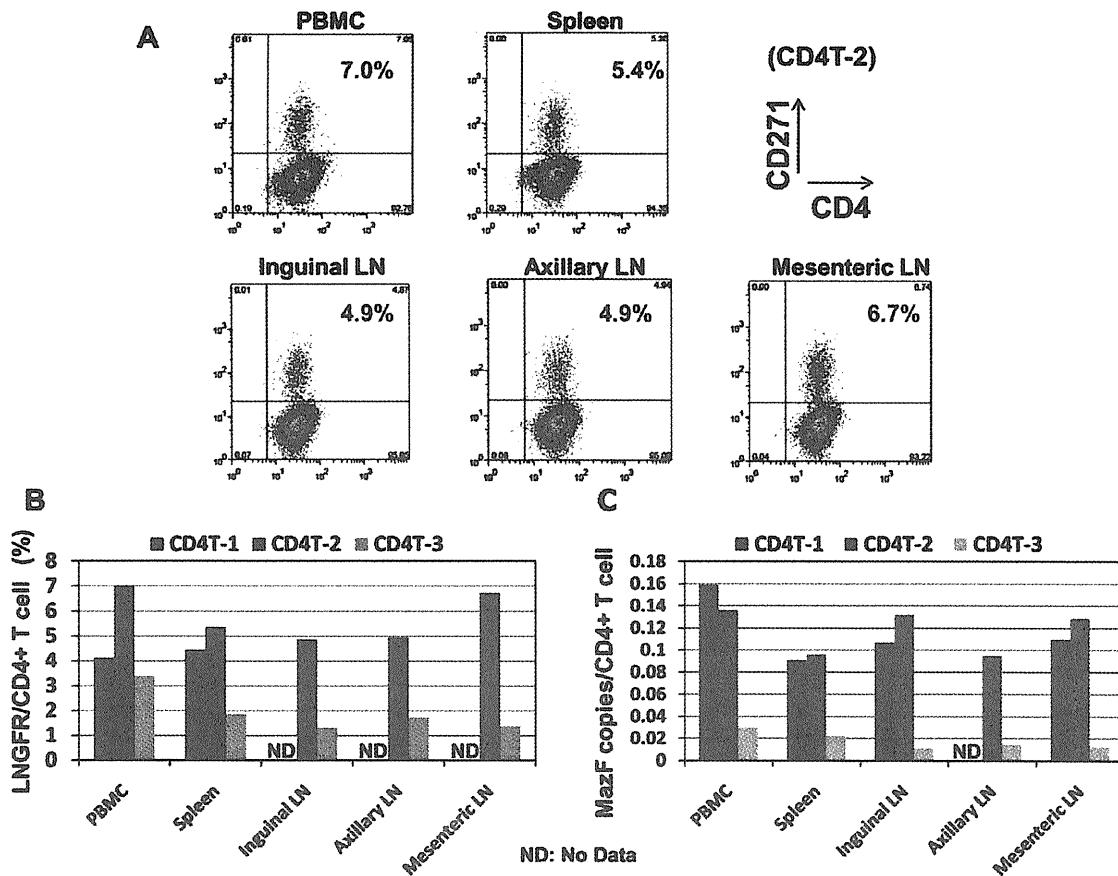


Figure 5. Analysis of the distribution of MazF-Tmac cells in several organs. (A) CD4+ T cells were isolated from lymphocytes separated from several organs, incubated 3–4 days, and stained with anti-CD4 and anti-CD271 antibodies. CD4T-2 is represented by a dot plot. (B) The percentage of CD271+ cells from three macaques is summarized. (C) The Copy number of the MazF gene in CD4+ T cells from each organ was calculated from real-time PCR and flow cytometric data.

doi:10.1371/journal.pone.0023585.g005

circulation has been observed following infusions of about 10 billion cells [17], and higher cell doses results in higher levels of engraftment [18,19]. Infusions of lower than 5×10^9 cells do not reliably result in measurable engraftment levels [19]. Therefore, we decided to infuse more than one billion cells into cynomolgus macaques, reflecting one-tenth of the scale of the human model. Indeed, the *mazF* gene-modified cells were detected over a six month period at a high level, and no histopathological disorders and no MazF-specific antibody production was observed during the experiment, demonstrating that MazF-Tmac cells showed little or no immunogenicity to monkeys. Moreover, MazF-Tmac cells harvested from the CD4T-1-transplanted monkey 6 months post-infusion showed resistance to the replication of SHIV 89.6P, indicating that the long-term persistent MazF-Tmac cells are functional. The expression of MazF in the SHIV-infected MazF-Tmac cells was below the limit of detection due to a low MOI such as 0.01, while in the MazF-Tmac cells transduced with the Tat expression retroviral vector M-LTR-Tat-ZG at 45% efficiency, expression of MazF was clearly induced, indicating that Tat dependent MazF expression system was maintained in the cells even 6 months after the autologous transplantation.

Because gene therapy for HIV is aimed at reconstituting an HIV-resistant immune system, genetically modified cells must

inhibit virus replication and maintain persistence *in vivo*. Although *ex vivo* gene therapy targeting CD4+ T cells or CD34+ hematopoietic stem cells has been shown to promote long term persistence of infused cells in peripheral blood in human, it is difficult to obtain information about the distribution pattern of these cells in the whole human body. In order to obtain such information, the monkeys were sacrificed and lymphocytes were isolated from several organs after 6 months of monitoring. Importantly, the infused MazF-Tmac cells were detected in secondary lymphoid tissue, such as several LNs and spleen, and in peripheral blood, although individual differences between CD4T-1, -2, and -3-transplanted monkeys were observed. No histopathological disorders were observed in the organs containing MazF-Tmac cells, indicating that there were no lesions relating to MazF-Tmac cells. The distribution of MazF-Tmac cells in the lymphoid tissues of CD4T-3-transplanted monkey was lower compared to the CD4T-1 and -2-transplanted monkeys. One reason for this phenomenon is likely the lower dosage of busulfan used to treat the CD4T-3-transplanted monkey. Busulfan is an alkylating agent with potent effects on hematopoietic stem cells that is commonly used for stem cell transplantation. In rhesus macaques, a low-dose of busulfan has an impact on bone marrow stem/progenitor cells with transient and mild suppression of peripheral blood counts

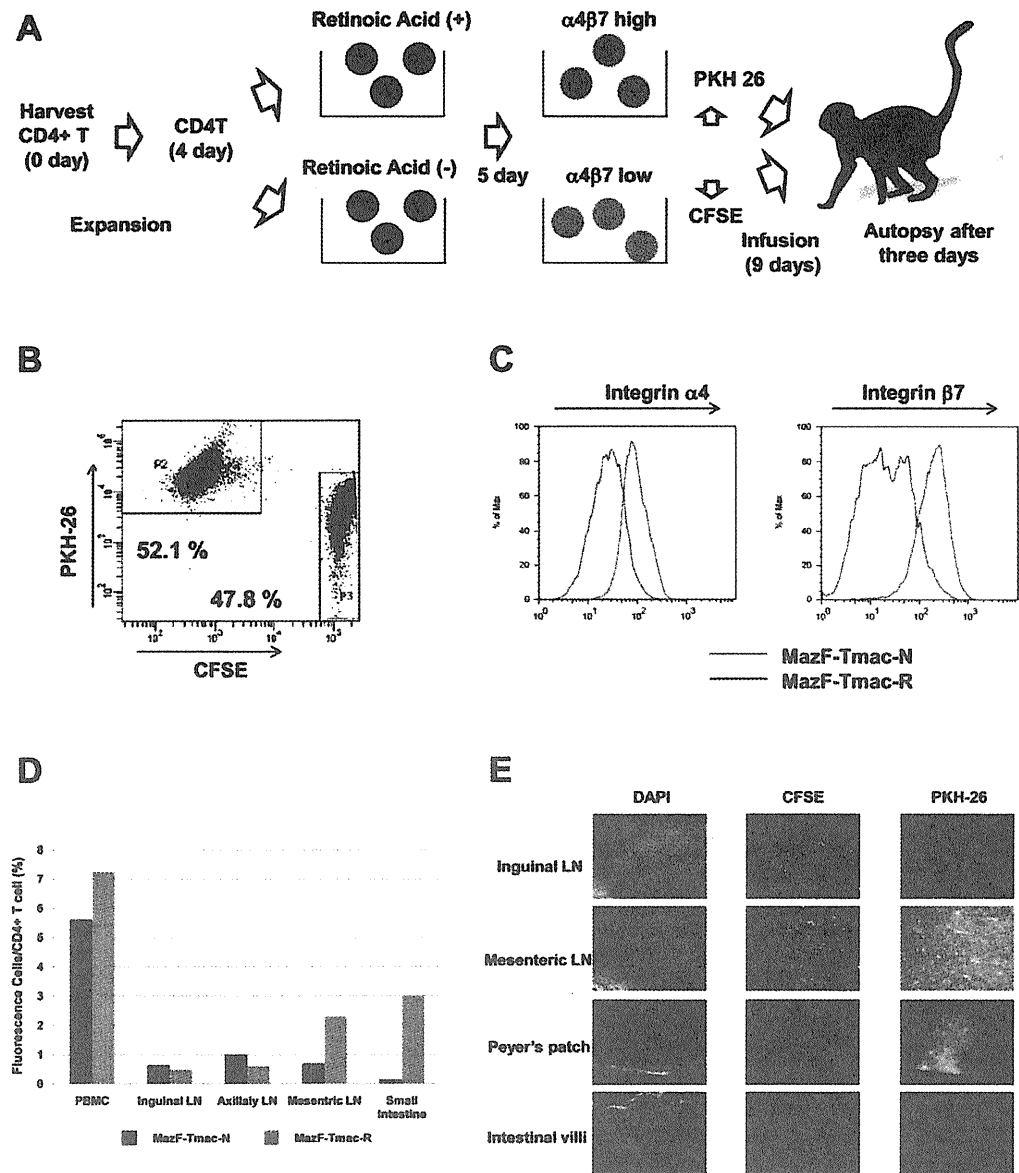


Figure 6. Comparison of the homing effect of MazF-Tmac cells treated with or without retinoic acid. (A) CD4⁺ T cells from the CD4T-4 monkey were stimulated with anti-CD3/CD28 beads, and MT-MFR-PL2 vector was transduced twice on days 3 and 4. After transduction, total lymphocytes were divided into two culture conditions in which retinoic acid was added to the one. After an additional 5 days of incubation, control and retinoic acid-treated cells were stained with CFSE and PKH26, respectively, mixed at nearly the same numbers, and infused into the autologous CD4T-4. Three days after the transplantation, experimental autopsy was performed. (B) A mixture of the two groups of MazF-Tmac cells stained with CFSE and PKH26 was analyzed using flow cytometry; the ratio of the two groups was almost same. (C) Up-regulation of the homing receptor was confirmed in the MazF-Tmac-R cells. The MazF-Tmac-N and MazF-Tmac-R cells are indicated by the blue line and red line, respectively. (D) Lymphocytes were collected from three lymph nodes (LNs) and small intestines, and a percentage of fluorescently-labeled cells were analyzed by flow cytometry. (E) Fluorescence microscope analysis of distal organ specimens.
doi:10.1371/journal.pone.0023585.g006

[20]. Thus, the lower engraftment efficiency of CD4T-3 (MazF-Tmac) cells might be due to the milder busulfan treatment.

In contrast to the LNs and spleen, a limited number of cells were detected in non-lymphoid tissues such as small intestine and liver. Considering HIV-1 infection, the gastrointestinal (GI) tract, which contains the vast majority of lymphoid tissues in the total body to protect mucosal membranes from foreign antigens, is the

dominant site of HIV replication rather than LNs, which were originally thought to be the main infection sites [21]. In GI tract, CD4⁺ T cells are dramatically decreased during the acute phase of HIV infection [21,22,23]. In rhesus macaques, a similar depletion was also reported during the acute phase of simian immunodeficiency virus (SIV) infection, with CD4⁺ memory T cells specifically targeted [24,25]. Notably, the rate of mucosal CD4⁺

T cell depletion in pathogenic SIV-infected monkeys correlates with the disease progression in the rhesus macaque [26]. Indeed, recent studies provide evidence that the depletion of mucosal CD4+ T cells leads to damage of the gut mucosal layer resulting in translocation of microbial products, such as lipopolysaccharide (LPS), ultimately causing chronic and systemic immune activation, which is one of the hallmarks of HIV/SIV infection and one of the predictors of disease progression [27,28]. Although HAART therapy is effective in controlling viral replication and recovering CD4+ T cells in the peripheral blood, restoration of CD4+ T cells is delayed in the GI tract [21,29]. Thus, the repair of depleted CD4+ T cells using gene therapy might attenuate the breakdown of the mucosal layer and prevent mucosal immune system deficiency. To change the tissue distribution of infused CD4+ T cells, the enhancement of homing receptor expression in T lymphocyte is necessary. Integrin $\alpha 4\beta 7$ is known to facilitate the migration of lymphocytes from gut-inductive sites where immune responses are first induced (Peyer's patches and mesenteric LNs) to the lamina propria [30,31]. Expression of the homing receptor is induced by the addition of retinoic acid [32], which is produced mainly from retinol (vitamin A) by dendritic cells in the mesenteric LNs. As shown in Figure 6D and 6E, although these are preliminary data with only one monkey, editing of the homing receptors integrin- $\alpha 4$ and integrin- $\beta 7$ by retinoic acid enhanced the recruitment of MazF-Tmac cells to the mesenteric LNs, small intestine, and Peyer's patches. These results may indicate that MazF-Tmac cells treated with retinoic acid selectively accumulate in the mesenteric LNs and then migrate into Peyer's patches. It has been reported that the HIV-1 envelope protein gp120 binds to and signals through the activated form of integrin $\alpha 4\beta 7$ [33]; however, we expect that retinoic acid-treated MazF-T cells will persist in distal organs without the additional spread of HIV replication because of the HIV-1 resistance observed in the MazF-Tmac cells. Therefore, we speculate that the combination of several culture methods to edit the homing receptor will enhance the recruitment of MazF-Tmac cells to distal lymphoid organs, resulting in a more efficient therapeutic.

In summary, we showed long-term persistence, safety and continuous HIV replication resistance in the *mazF* gene-modified CD4+ T cells in a non-human primate model *in vivo*, suggesting that autologous transplantation of *mazF* gene-modified cells is an attractive strategy for HIV gene therapy.

Materials and Methods

Vector design and viral production

The GALV-enveloped gamma retroviral vector MT-MFR-LP2 was generated as previously described [6]. MT-MFR-PL2 expresses a truncated form of the human low affinity nerve growth factor gene (Δ LNGFR) [34] under the control of a functional PGK promoter and the MazF gene under control of the HIV-LTR promoter (Figure 1A). The Δ LNGFR is a surface marker that allows identification of transduced cells.

Animals

Four cynomolgus macaques (*Macaca fascicularis*, 6–7 years old), CD4T-1, CD4T-2, CD4T-3, and CD4T-4, were used in this experiment and were maintained at the Tsukuba Primate Research Center for Medical Science at the National Institute of Biomedical Innovation (NIBIO, Ibaraki, Japan). The study was conducted according to the Rules for Animal Care and the Guiding Principles for Animal Experiments Using Nonhuman Primates formulated by the Primate Society of Japan [35] and in accordance with the recommendations of the Weatherall report,

“The use of non-human primates in research”. The protocols for the experimental procedures were approved by the Animal Welfare and Animal Care Committee of the National Institute of Biomedical Innovation (DS18-100). All surgical and invasive clinical procedures were conducted by trained personnel under the supervision of a veterinarian in a surgical facility using aseptic techniques and comprehensive physiologic monitoring. Ketamine hydrochloride (Ketalar, 10 mg/kg; Daichi-Sankyo, Tokyo, Japan) was used to induce anesthesia for all clinical procedures associated with the study protocol such as blood sampling, gene-modified cell administration, clinical examinations and treatment.

Ex vivo expansion of CD4+ T cells, and transduction of the MazF vector

Peripheral blood from cynomolgus macaques was collected by apheresis as previously described [36]. For the dissolution of red blood lymphocytes, collected blood was treated with ACK lysing buffer (Lonza, Walkersville, MD) and was washed twice with phosphate buffered saline (PBS). Then, CD4+ T cells were isolated using anti-CD4 conjugated magnetic beads (DynaL CD4 Positive Isolation Kit, Invitrogen, Carlsbad, CA) according to the manufacturer's instructions. Isolated CD4+ T cells were cultured at 5×10^5 cells/ml in GT-T503 (Takara Bio, Otsu, Japan) supplemented with 10% FBS (Invitrogen), 200 IU recombinant human interleukin-2 (IL-2; Chiron, Emeryville, CA), 2 mM L-glutamine (Lonza), 2.5 μ g/ml Fungizone (Bristol Myers-Squibb, Woerden, The Netherlands) and activated for three days with either 5 μ g/ml concanavalin A (Con A, Sigma Chemical, St. Louis, MO) for CD4T-1 or a combination of anti-CD3 clone FN-18 (Biosource, Camarillo, CA, USA) and anti-CD28 clone L293 (BD Biosciences, Franklin Lakes, NJ) monoclonal antibodies conjugated to M-450 epoxy magnetic beads (Invitrogen) at cell-to-bead ratio of 1:1 (CD4T-2 and CD4T-3). On day 3, the activated CD4+ T cells were transduced with the MazF retroviral vector MT-MFR-PL2 in the presence of RetroNectin[®] (Takara Bio) according to manufacturer's instructions. Transduction was repeated on day 4. CD4+ T cells were further expanded to day 7 to 9 until the total cell number reach more than 10^9 . The closed system MazF-Tmac cell manufacturing was performed using gas permeable culture bags; CultiLife 215 (Takara Bio) and CultiLife Eva (Takara Bio) were used for CD4+ T cells expansion and CultiLife spin (Takara Bio) was used for transduction of the MazF retroviral vector.

Transplantation of expanded CD4+ T cells

Prior to the transplantation, each macaque was treated with busulfan (Ohara Pharmaceutical, Shiga, Japan). Busulfan has been used extensively as a preparatory regimen for allogeneic hematopoietic stem cell transplantation based on its toxicity to hematopoietic stem cells. Furthermore, it has been reported that in non-human primates, hematopoiesis was significantly decreased after a single, clinically well-tolerated dose of busulfan, with slow, but almost complete, recovery over the next several months [20]. The effects of busulfan on lymphocyte engraftment, however, are not well documented. Although cyclophosphamide is widely used in immune gene therapy trials in humans for lymphocyte transplantation, there is no information available for cyclophosphamide effect on T-cell transplantation in the cynomolgus macaque. It should be noted that we have chosen busulfan for our CD4+ T cell transplantation because busulfan is shown to cause a reduction in the peripheral blood count in human trial [37], we have had success in using busulfan for cynomolgus macaque bone marrow transplantation and according to internal information, busulfan causes a reduction of the peripheral blood count in

cynomolgus macaques. Busulfan was orally administered to the macaques twice at 10 mg/kg each (CD4T-1 and CD4T-2) or 6 mg/kg each (CD4T-3) [38]. The expanded cells were harvested, washed three times with PBS, and re-suspended in PBS containing 10% autologous plasma. The collected cells were infused intravenously to monkeys at the speed of 1 ml per minute.

Flow cytometry analysis

The cell surface markers of the expanded cells and peripheral blood mononuclear cells (PBMC) were analyzed using FACSCalibur (BD Bioscience) and FACSCanto (BD Bioscience), and data analysis was performed using CellQuest software (BD Bioscience), FACSDiva software (BD Bioscience) or FlowJo software (Tree Star, Inc., Ashland, OR). The following antibodies were used for staining: anti-CD3 (SP34-2, PerCP), anti-CD4 (L200, FITC), anti-CD25 (2A3, FITC), anti-CD28 (CD28.2, PE), anti-CD95 (DX2, FITC), anti-CXCR4 (12G5, PE) and anti-integrin- β 7 (FIB504, PE), which were obtained from BD Bioscience. The anti-CD49d (HP2/1, FITC) antibody was obtained from Beckman Coulter (Fullerton, CA), and the anti-CD271 (LNGFR, PE and APC) antibodies were obtained from Miltenyi Biotec GmbH (Bergisch Gladbach, Germany).

Measurement of hematological data

Two ml of blood was prepared every week. Blood samples were used to measure the white blood cell (WBC) count, red blood cell (RBC) count, hemoglobin (Hb) concentration, hematocrit value, mean corpuscular volume, mean cell hemoglobin concentration and platelet (PLT) count using a Sysmex K-4500 instrument (Toa-iyoudenshi, Kobe, Japan). The concentrations of the biochemical markers in blood samples were also monitored including total proteins, albumin, blood urea nitrogen, glucose, glutamic oxaloacetic transaminase, glutamic pyruvic transaminase, alkaline phosphatase, creatine phosphokinase, lactate dehydrogenase, creatine, sodium, potassium, chlorine and C-reactive protein using an AU400 instrument (Olympus Medical Systems, Tokyo, Japan).

Quantification of gene-modified CD4+ T cells

The existence and persistence of genetically modified CD4+ T cells were monitored by measuring the proviral genome of the transgene using quantitative real-time PCR. DNA samples were extracted from 2×10^6 PBMCs using a Genra Puregene Blood Kit (QIAGEN, Hilden, Germany). The proviral copy number of the transgene was calculated from 400 ng of genomic DNA with quantitative PCR using a Cycleave RT-PCR Core Kit (Takara Bio) and Provirus Copy Number Detection Primer Set (Takara Bio) according to the manufacturer's instructions. The reaction was performed with the Thermal Cycler Dice Real Time System (Takara Bio), and the data was analyzed using Multiplate RQ software (Takara Bio). For each run, a standard curve was generated from the pMT-MFR-PL2 plasmid, whose copy numbers were already known. Based on the standard curve, the amount of infused cells was quantified.

Detection of anti-MazF antibodies in macaque blood after transplantation of MazF-Tmac cells

To examine whether anti-MazF antibodies can be generated after the transplantation of MazF-Tmac cells, the plasma isolated from the macaques was analyzed. In order to detect anti-MazF antibodies, purified MazF protein or anti-monkey IgG (Nordic Immunological Laboratories, Tilburg, The Netherlands) was pre-coated onto the wells of a 96-well microplate and subsequently

blocked with PBS-1% BSA. The plasma samples were isolated from the CD4T-2 at day 0, 33, 75, and 103 after transplantation and were diluted to 500,000-fold, 50,000-fold, and 10,000-fold. Cynomolgus macaque IgG purified from normal macaque plasma with Melon Gel IgG purification Kit (Thermo Fisher Scientific, Rockford, IL, USA) was used as a control for this reaction. The two-fold serial dilutions of the IgG (1 ng/ml to 64 ng/ml) and the diluted plasma samples, as described above, were separately added to each well. After an overnight incubation at 4°C, the wells were washed with PBS-1% BSA. The POD-conjugated anti-monkey IgG (Nordic Immunological Laboratories) was then added to the wells. After 4 hours of incubation at room temperature, the wells were washed three times with PBS-1% BSA followed by the addition of the substrate solution (o-Phenylenediamine, Sigma). The optical density of each well was read at 490/650 nm using a 680XR microplate reader (Bio-Rad Laboratories, Hercules, CA) after stopping the reaction with H₂SO₄ stop solution (Figure S1).

Examination of the anti-viral efficacy of MazF-Tmac cells harvested from a monkey

To examine the function of the *mazF* gene in cells harvested from a MazF-Tmac-transplanted monkey, the frozen lymphoid cells from CD4T-1 at autopsy (214 days post-infusion of MazF-Tmac cells) were recovered, CD4+ T cells were selected using a CD4+ T Cell Isolation Kit (Miltenyi Biotec), stimulated with anti-CD3/CD28 beads at a cell-to-bead ratio of 1:1, and expanded in GT-T503 medium supplemented with 10% FBS, 200 IU recombinant human interleukin-2, 2 mM L-glutamine, 2.5 μ g/ml Fungizone, 100 units/ml penicillin, and 100 μ g/ml streptomycin. After 7 days of expansion, the genetically modified cells expressing Δ LNGFR+ were concentrated with an anti-CD271 monoclonal antibody (CD271 MicroBeads, Miltenyi Biotec) and expanded for 4 days. The cells from the CD271-negative fraction were also harvested and expanded as control non-gene modified CD4+ T cells. The expanded CD271-enriched cells and CD271-negative cells were infected with SHIV 89.6P at the MOI of 0.01 and cultured for 6 more days. Culture supernatants and cell pellets were harvested at 6 days post-infection. RNA in the culture supernatant was recovered with the QIAamp Viral RNA Mini Kit (QIAGEN) and SHIV RNA levels in the culture supernatant were determined by quantitative real-time PCR with a set of specific primers specific for the SHIV *gag* region [39]. In order to detect the Tat-dependent expression of MazF in the CD271-enriched MazF-Tmac cells harvested from the monkey, the cells were transduced with the Tat expression retroviral vector M-LTR-Tat-ZG [6] in the presence of RetroNectin[®] as per the manufacturer's instruction. Twenty hours after Tat transduction, the cells were harvested, counted by trypan blue exclusion assay, washed twice with PBS, and 5×10^5 cells were suspended in 50 μ l of 1 \times SDS sample buffer. The cell samples were incubated at 95°C for 10 min, and 5 μ l of each cell sample was used for western blot analysis. For gel electrophoresis of proteins, the sample solutions described above were loaded into the wells of a 4–20% Tris-Glycine gel (Atto, Tokyo, Japan). After completion of electrophoresis, the gel was transferred to a polyvinylidene fluoride (PVDF) membrane (Millipore, Billerica, MA) with papers containing transfer buffer using the semi-dry method at 60 mA (constant voltage) for 60 min. The membrane was cut in half horizontally around the 20 kDa protein band of the pre-stained protein marker (Bio-Rad Laboratories). The upper part of the membrane was used to detect the α -tubulin (50 kDa) as an internal standard, while the lower part of the membrane was used to detect MazF (12 kDa). After blocking, the membranes were then incubated overnight at 4°C in the blocking buffer (5% skim milk in PBS)

containing 1 µg/ml anti- α -tubulin antibody (Cell Signaling Technology) and 1 µg/ml anti-MazF polyclonal antibody (rabbit, in-house preparation), respectively. Each membrane was washed three times and subsequently incubated at room temperature for 1 hour in 10 ml of the blocking buffer containing the 10,000-fold diluted goat anti-IgG rabbit antibody (peroxidase conjugated, Thermo Fisher Scientific). The membrane was washed five times by gentle shaking in the washing buffer at room temperature for 5 min. The membrane was soaked at room temperature for 5 min in substrate solution (SuperSignal West Femto Maximum Sensitivity Chemiluminescent Substrate, Thermo Scientific). Protein signals were detected by a CCD camera (LuminoShot 400 Jr, Takara Bio), which captures a digital image of the western blot.

Collection of lymphocyte from several organs

Several organs were collected following euthanasia of the monkeys. After thoracotomy, the right atrium was incised, and 2 L of heparinized PBS was infused into the left ventricle using an 18-gauge needle. After perfusion, several organs were collected, and lymphocytes were separated using the following method: samples of spleen, thymus, liver, bone marrow, and axillary, inguinal and mesenteric LNs were minced and filtered through a 40 µm nylon filter (BD Bioscience); lymphocyte of the small intestine were collected by the Percoll (GE Healthcare, Castle Hill, Australia) density-gradient centrifugation method as described previously [39]; and lymphocytes obtained from each organ were used for the flow cytometric analysis, and extracted DNA was used for quantification PCR.

In vivo homing analysis

CD4T-4 was used for homing analysis. Isolated CD4+ T cells were stimulated with anti-CD3/CD28 beads and cultured in GT-T503 medium supplemented with 10% FBS, 200 IU IL-2, 2 mM L-glutamine, and 2.5 µg/ml Fungizone. After 4 days of expansion, activated CD4+ T cells were divided into two culture bags (ClutiLife Eva), and 10 nM retinoic acid (Sigma) was added to one of the bags. After an additional 5 days of incubation, expanded cells with or without retinoic acid were harvested and labeled with 2 mM PKH26 (Sigma) or 5 µM CFSE (Sigma), respectively,

according to the manufacturer's instructions. Thereafter, the cells were washed three times with PBS, mixed in PBS containing 10% autologous plasma and infused into the macaque. Then, CD4T-4 was euthanized at 3 days after transplantation. Lymphocytes from several organs were collected as previously described, and the distributions of labeled lymphocytes were detected by flow cytometric analysis. The specimens from several organs were fixed in buffered formaldehyde and embedded in plastic. Serial sections were made using a diamond saw. The slides were then analyzed under a fluorescence microscope to detect the distribution of the expanded cells in the distal organ specimens.

Supporting Information

Figure S1 Raw data of 490/650 nm absorbance. The raw data of the optical density of each well at 490/650 nm was read using a microplate reader 680XR (Bio-Rad Laboratories, Hercules, CA) is represented.

(PDF)

Figure S2 Photographs of histopathological analysis. Individual photographic data of histopathological analysis of CD4T-1, -2, and -3 in Table 3 is represented.

(PDF)

Acknowledgments

The authors thank the staff of Tsukuba Primate Research Center and Corporation for Production and Research of Laboratory Primates for the kind care and expert handling of the animals. The authors also thank Dr. Keith A. Reimann of Harvard Medical School and Dr. Tomoyuki Miura of Kyoto University for providing the SHIV 89.6P. The authors are also grateful to Dr. Koich Inoue of Takara Bio Inc. for his critical reading of this manuscript and Tomomi Sakuraba of Takara Bio Inc. for conducting the quantitative PCR assay.

Author Contributions

Conceived and designed the experiments: HC NS YY KT JM IK. Performed the experiments: HC NS HT HS NA. Analyzed the data: HC NS HS NA. Contributed reagents/materials/analysis tools: NS HT HS NA. Wrote the paper: HC NS.

References

- Panel on Antiretroviral Guidelines for Adults and Adolescents. Guidelines for the use of antiretroviral agents in HIV-1-infected adults and adolescents. Department of Health and Human Services. December 1, 2009; 1–161. <http://www.aidsinfo.nih.gov/ContentFiles/AdultandAdolescentGL.pdf>. Accessed September 16, 2010.
- Sarver N, Rossi J (1993) Gene therapy: a bold direction for HIV-1 treatment. *AIDS Res Hum Retroviruses* 9: 483–487.
- Dropulic B, Jeang KT (1994) Gene therapy for human immunodeficiency virus infection: genetic antiviral strategies and targets for intervention. *Hum Gene Ther* 5: 927–939.
- Dropulic B, June CH (2006) Gene-based immunotherapy for human immunodeficiency virus infection and acquired immunodeficiency syndrome. *Hum Gene Ther* 17: 577–588.
- Rossi JJ, June CH, Kohn DB (2007) Genetic therapies against HIV. *Nat Biotechnol* 25: 1444–1454.
- Chono H, Matsumoto K, Tsuda H, Saito N, Lee K, et al. (2011) Acquisition of HIV-1 Resistance in T Lymphocytes Using an ACA-specific *E. coli* mRNA interferase. *Hum Gene Ther* 22: 1–9.
- Onlamoon N, Hudson K, Bryan P, Mayne AE, Bonyhadi M, et al. (2006) Optimization of *in vitro* expansion of macaque CD4 T cells using anti-CD3 and co-stimulation for autotransfusion therapy. *J Med Primatol* 35: 178–193.
- Onlamoon N, Plagnan N, Rogers KA, Mayne AE, Bostik P, et al. (2007) Anti-CD3/28 mediated expansion of macaque CD4+ T cells is polyclonal and provides extended survival after adoptive transfer. *J Med Primatol* 36: 206–218.
- Pitcher CJ, Hagen SI, Walker JM, Lam R, Mitchell BL, et al. (2002) Development and homeostasis of T cell memory in rhesus macaque. *J Immunol* 168: 29–43.
- Klebanoff CA, Gattinoni L, Torabi-Parizi P, Kerstann K, Cardones AR, et al. (2005) Central memory self/tumor-reactive CD8+ T cells confer superior antitumor immunity compared with effector memory T cells. *Proc Natl Acad Sci U S A* 102: 9571–9576.
- Reimann KA, Li JT, Voss G, Lekutis C, Tenner-Racz K, et al. (1996) An env gene derived from a primary human immunodeficiency virus type 1 isolate confers high *in vivo* replicative capacity to a chimeric simian/human immunodeficiency virus in rhesus monkeys. *J Virol* 70: 3198–3206.
- Engelberg-Kulka H, Hazan R, Amitai S (2005) *mazEF*: a chromosomal toxin-antitoxin module that triggers programmed cell death in bacteria. *J Cell Sci* 118: 4327–4332.
- Zhang Y, Zhang J, Hoeflich KP, Ikura M, Qing G, et al. (2003) MazF cleaves cellular mRNAs specifically at ACA to block protein synthesis in *Escherichia coli*. *Mol Cell* 12: 913–923.
- Suzuki M, Zhang J, Liu M, Woychik NA, Inouye M (2005) Single protein production in living cells facilitated by an mRNA interferase. *Mol Cell* 18: 253–261.
- Baik S, Inoue K, Ouyang M, Inouye M (2009) Significant bias against the ACA triplet in the tmRNA sequence of *Escherichia coli* K-12. *J Bacteriol* 191: 6157–6166.
- Shimazu T, Degenhardt K, Nur-E-Kamal A, Zhang J, Yoshida T, et al. (2007) NBK/BIK antagonizes MCL-1 and BCL-XL and activates BAK-mediated apoptosis in response to protein synthesis inhibition. *Genes Dev* 21: 929–941.
- Levine BL, Humeau LM, Boyer J, MacGregor RR, Rebello T, et al. (2006) Gene transfer in humans using a conditionally replicating lentiviral vector. *Proc Natl Acad Sci U S A* 103: 17372–17377.
- Ranga U, Woffendin C, Verma S, Xu L, June CH, et al. (1998) Enhanced T cell engraftment after retroviral delivery of an antiviral gene in HIV-infected individuals. *Proc Natl Acad Sci U S A* 95: 1201–1206.

19. van Lunzen J, Glaunsinger T, Stahmer I, von Baehr V, Baum C, et al. (2007) Transfer of autologous gene-modified T cells in HIV-infected patients with advanced immunodeficiency and drug-resistant virus. *Mol Ther* 15: 1024–1033.
20. Kuramoto K, Follman D, Hematti P, Sellers S, Laukkanen MO, et al. (2004) The impact of low-dose busulfan on clonal dynamics in nonhuman primates. *Blood* 104: 1273–1280.
21. Brechley JM, Schacker TW, Ruff LE, Price DA, Taylor JH, et al. (2004) CD4+ T cell depletion during all stages of HIV disease occurs predominantly in the gastrointestinal tract. *J Exp Med* 200: 749–759.
22. Guadalupe M, Reay E, Sankaran S, Prindiville T, Flamm J, et al. (2003) Severe CD4+ T-cell depletion in gut lymphoid tissue during primary human immunodeficiency virus type 1 infection and substantial delay in restoration following highly active antiretroviral therapy. *J Virol* 77: 11708–11717.
23. Mehandru S, Poles MA, Tenner-Racz K, Horowitz A, Hurley A, et al. (2004) Primary HIV-1 infection is associated with preferential depletion of CD4+ T lymphocytes from effector sites in the gastrointestinal tract. *J Exp Med* 200: 761–770.
24. Mattapallil JJ, Douek DC, Hill B, Nishimura Y, Martin M, et al. (2005) Massive infection and loss of memory CD4+ T cells in multiple tissues during acute SIV infection. *Nature* 434: 1093–1097.
25. Li Q, Duan L, Estes JD, Ma ZM, Rourke T, et al. (2005) Peak SIV replication in resting memory CD4+ T cells depletes gut lamina propria CD4+ T cells. *Nature* 434: 1148–1152.
26. Picker LJ, Hagen SI, Lum R, Reed-Inderbitzin EF, Daly LM, et al. (2004) Insufficient production and tissue delivery of CD4+ memory T cells in rapidly progressive simian immunodeficiency virus infection. *J Exp Med* 200: 1299–314.
27. Brechley JM, Price DA, Schacker TW, Asher TE, Silvestri G, et al. (2006) Microbial translocation is a cause of systemic immune activation in chronic HIV infection. *Nat Med* 12: 1365–1371.
28. Estes JD, Harris LD, Klatt NR, Tabb B, Pittaluga S, et al. (2010) Damaged intestinal epithelial integrity linked to microbial translocation in pathogenic simian immunodeficiency virus infections. *PLoS Pathog* 2010 Aug 19;6(8): pii: e1001052. PubMed PMID: 20808901.
29. Guadalupe M, Sankaran S, George MD, Reay E, Verhoeven D, et al. (2006) Viral suppression and immune restoration in the gastrointestinal mucosa of human immunodeficiency virus type 1-infected patients initiating therapy during primary or chronic infection. *J Virol* 80: 8236–8247.
30. von Andrian UH, Mackay CR (2000) T-cell function and migration. Two sides of the same coin. *N Engl J Med* 343: 1020–1034.
31. Wagner N, Löhler J, Kunkel EJ, Ley K, Leung E, et al. (1996) Critical role for beta7 integrins in formation of the gut-associated lymphoid tissue. *Nature* 382: 366–370.
32. iwata M, Hirakiyama A, Eshima Y, Kagechika H, Kato C, et al. (2004) Retinoic acid imprints gut-homing specificity on T cells. *Immunity* 21: 527–538.
33. Arthos J, Cicala C, Martinelli E, Macleod K, Van Ryk D, et al. (2008) HIV-1 envelope protein binds to and signals through integrin alpha4beta7, the gut mucosal homing receptor for peripheral T cells. *Nat Immunol* 9: 301–309.
34. Verzeletti S, Bonini C, Markt S, Nobili N, Cicri F, et al. (1998) Herpes simplex virus thymidine kinase gene transfer for controlled graft-versus-host disease and graft-versus-leukemia: clinical follow-up and improved new vectors. *Hum Gene Ther* 9: 2243–2251.
35. Primate Society of Japan (1986) Guiding principles for animal experiments using nonhuman primates. *Primate Res* 2: 111–113.
36. Ageyama N, Kimikawa M, Eguchi K, Ono F, Shibata H, et al. (2003) Modification of the leukapheresis procedure for use in rhesus monkeys (*Macaca mulata*). *J Clin Apher* 18: 26–31.
37. Laurent J, Speiser DE, Appay V, Touvrey C, Vicari M, et al. (2010) Impact of 3 different short-term chemotherapy regimens on lymphocyte-depletion and reconstitution in melanoma patients. *J Immunother* 33: 723–734.
38. Masuda S, Ageyama N, Shibata H, Obara Y, Ikeda T, et al. (2009) Cotransplantation with MSCs improves engraftment of HSCs after autologous intra-bone marrow transplantation in nonhuman primates. *Exp Hematol* 37: 1250–1257.
39. Miyake A, Ibuki K, Enose Y, Suzuki H, Horiuchi R, et al. (2006) Rapid dissemination of a pathogenic simian/human immunodeficiency virus to systemic organs and active replication in lymphoid tissues following intrarectal infection. *J Gen Virol* 87: 1311–1320.

Spatial Configuration of Hepatitis E Virus Antigenic Domain[∇]

Li Xing,^{1,2†} Joseph C. Wang,^{1†} Tian-Cheng Li,³ Yasuhiro Yasutomi,⁴ James Lara,⁵ Yury Khudyakov,⁵ Darren Schofield,⁶ Suzanne U. Emerson,⁶ Robert H. Purcell,⁶ Naokazu Takeda,³ Tatsuo Miyamura,³ and R. Holland Cheng^{1*}

Molecular and Cellular Biology, University of California, Davis, California 95616¹; Karolinska Institute Structural Virology, F68 University Hospital, SE-14186 Stockholm, Sweden²; Department of Virology II, National Institute of Infectious Disease, Tokyo 162, Japan³; Tsukuba Primate Research Center, National Institute of Biomedical Innovation, Ibaraki 305-0843, Japan⁴; Division of Viral Hepatitis, Centers for Disease Control and Prevention (CDC), Atlanta, Georgia 30333⁵; and Hepatitis Virus Section, National Institute of Allergy and Infectious Diseases, Bethesda, Maryland 20892⁶

Received 26 March 2010/Accepted 28 October 2010

Hepatitis E virus (HEV) is a human pathogen that causes acute hepatitis. When an HEV capsid protein containing a 52-amino-acid deletion at the C terminus and a 111-amino-acid deletion at the N terminus is expressed in insect cells, the recombinant HEV capsid protein can self-assemble into a T=1 virus-like particle (VLP) that retains the antigenicity of the native HEV virion. In this study, we used cryoelectron microscopy and image reconstruction to show that anti-HEV monoclonal antibodies bind to the protruding domain of the capsid protein at the lateral side of the spikes. Molecular docking of the HEV VLP crystal structure revealed that Fab224 covered three surface loops of the recombinant truncated second open reading frame (ORF2) protein (PORF2) at the top part of the spike. We also determined the structure of a chimeric HEV VLP and located the inserted B-cell tag, an epitope of 11 amino acids coupled to the C-terminal end of the recombinant ORF2 protein. The binding site of Fab224 appeared to be distinct from the location of the inserted B-cell tag, suggesting that the chimeric VLP could elicit immunity against both HEV and an inserted foreign epitope. Therefore, the T=1 HEV VLP is a novel delivery system for displaying foreign epitopes at the VLP surface in order to induce antibodies against both HEV and the inserted epitope.

Hepatitis E virus (HEV) is a causative agent of acute hepatitis in humans and is primarily transmitted via the fecal-oral route. HEV is thus resistant to the low pH and digestive enzymes associated with the stomach and gastrointestinal tract. HEV regularly causes epidemics in many tropical and subtropical countries. In India, 101 outbreaks were confirmed by serological analysis in the state of Maharashtra in the last 5 years (6), and the lifetime risk of HEV infection exceeds 60% (28). Sporadic cases have also been reported in regions where HEV is endemic, as well as in areas where it is not endemic. Although some of these cases were associated with travel, many cases involved patients without a history of travel to regions where HEV is endemic. Accumulating evidence suggests that sporadic infection occurs through a zoonotic route and is not limited to developing countries. Seroprevalence suggests hepatitis E infection may also be prevalent in high-income countries (21), such as the United States (17), the United Kingdom (3), and Japan (18). The overall mortality rate of HEV infection during an outbreak generally ranges from 1 to 15%, and the highest mortality occurs in pregnant women, with fatality rates of up to 30% (19).

The HEV virion is composed of a 7.2-kb single-stranded RNA molecule and a 32- to 34-nm icosahedral capsid. The HEV genome contains three open reading frames (ORFs).

The capsid protein, encoded by the second open reading frame (ORF2), located at the 3' terminus of the genome, comprises 660 amino acids and is responsible for most capsid-related functions, such as assembly, host interaction, and immunogenicity. Recombinant ORF2 proteins can induce antibodies that block HEV infection in nonhuman primates (12, 27). Four major antigenic domains were predicted to be located within the C-terminal 268 amino acids of the ORF2 protein; one domain was experimentally identified as a neutralization epitope in the Sar-55 ORF2 capsid protein (25, 26). However, the minimal peptide needed to induce anti-HEV neutralizing antibodies contains residues 459 to 607 of the ORF2 protein (33), which is much longer than a linear antigenic epitope, suggesting that the neutralization epitope is conformational. Therefore, the detailed structure of the HEV capsid protein is required in order to understand the organization of HEV epitopes.

Currently, there are 1,600 HEV genomic sequences available through the International Nucleotide Sequence Database Collaboration. They are classified into four genotypes which vary by geographic distribution and host range (10). In contrast, only a single serotype has been identified, suggesting that the immunodominant domain of HEV is highly conserved among genotypes. Antibodies from any one of the four genotypes cross-react with the capsid protein of genotype 1 (7).

Like other hepatitis viruses, HEV does not propagate well in currently available cell culture systems. Hepatitis E preventive strategies so far rely on the use of ORF2-derived recombinant protein (16). When expressed in insect cells, recombinant truncated ORF2 protein (PORF2), with 52 residues deleted from

* Corresponding author. Mailing address: Molecular and Cellular Biology, University of California, 1 Shields Ave., Davis, CA 95616. Phone: (530) 752-5659. Fax: (530) 752-3085. E-mail: rhch@ucdavis.edu.

† These authors contributed equally.

∇ Published ahead of print on 10 November 2010.

the C terminus and 111 residues deleted from the N terminus, self-assembles into virus-like particles (VLPs) (15). Our previous structural analysis of recombinant HEV VLP by cryoelectron microscopy (cryo-EM) provided the first understanding of the quaternary arrangement of PORF2.

The essential assembly element of the PORF2 protein contained amino acids 125 to 600 (13), and the reconstructed VLP displayed a T=1 icosahedral particle composed of 60 copies of truncated PORF2 (30). Recently, crystal structures were reported for genotype 1 T=1 VLPs (31), genotype 3 T=1 VLPs (32), and genotype 4 T=1 VLPs (8), revealing that PORF2 is composed of three domains, the S domain, M domain, and P domain. The T=1 icosahedral shell is composed of 60 copies of S domains, while the M domain binds tightly to the S domain and interacts with two 3-fold-related M domains to form a surface plateau at each of the 3-fold axes. Two P domains are tightly associated as a dimeric spike that protrudes from each of the icosahedral 2-fold axes. As a result, on a low-resolution cryo-EM density map, the HEV T=1 VLP appears as an icosahedral particle with 30 spikes (30).

Although these VLPs are smaller (270 Å in diameter) than the native HEV virion (320 to 340 Å), oral administration of HEV VLPs to experimental animals can induce anti-HEV antibodies that bind to native HEV (14). When a B-cell tag of 11 amino acids on glycoprotein D of herpes simplex virus was covalently coupled to the C-terminal end of PORF2 (after residue 608), the fusion protein retained the ability of PORF2 to assemble and form chimeric T=1 icosahedral VLPs that were capable of eliciting systemic and mucosal antibodies against both HEV capsid protein and the attached B-cell tag (20). Therefore, the HEV T=1 VLP is a potential carrier for delivering not only HEV antigen but also foreign antigens or antiviral drugs to the host immune system. However, rational design of HEV-based delivery vectors requires detailed information on HEV VLP structure, as well as on HEV immunodominant domains.

Here, we identified antigenic structures using cryo-EM and three-dimensional reconstruction. Our results indicate that the binding footprint of a neutralizing antibody covers the lateral side of the P domain, while a B-cell tag at the C terminus does not alter the assembly of T=1 HEV VLP.

MATERIALS AND METHODS

Production and purification of anti-HEV monoclonal antibody (MAb) MAb224. Eight-week-old female BALB/c mice were immunized at 0 and 4 weeks by intraperitoneal inoculation with HEV VLPs (100 µg/ml). Four weeks later, a final boost containing an equal volume of antigen was administered. Three days after the final boost, mouse spleen cells were fused with P3U1 mouse myeloma cells using polyethylene glycol 1500 (50% [wt/vol]) (Boehringer, Mannheim, Germany) essentially as described by Adler and Faine (1). Supernatants from microplate wells positive for hybridoma growth were screened by enzyme-linked immunosorbent assay (ELISA) using recombinant HEV VLPs as the antigen. Hybridomas that secrete antibodies specific for HEV were subcloned three times by limiting dilution, after which they were considered to be monoclonal. Antibodies in the supernatants were isotyped using a mouse monoclonal antibody isotyping kit (Amersham, Little Chalfont, Buckinghamshire, United Kingdom) in accordance with the manufacturer's protocol. Hybridomas were grown in bulk in stationary flasks (Nunc, Roskilde, Denmark) using RPMI 1640 with 15% fetal calf serum. Antibodies were purified from cell supernatants using HiTrap protein G affinity columns (Pharmacia Biotech AB, Uppsala, Sweden) and stored at -80°C. Among all of the antibodies that were generated, MAb224, an immunoglobulin G1 (IgG1) isotype, was chosen for structural analysis.

Preparation of Fab224 fragments. Isolated Fab224 fragments were prepared from purified mouse monoclonal antibodies by papain cleavage. A reducing L-cysteine buffer was used to activate the papain, and MAb224 was mixed with papain at a molar ratio of 100:1. The mixture was incubated overnight at 30°C. The reaction was stopped by the addition of iodoacetamide, and the product was analyzed by SDS-PAGE. The Fab224 fragments were purified using a 5-ml prepacked protein A chromatography column (Pierce Protein Research) according to the manufacturer's instructions. The Fc fragments and uncleaved MAb224 antibodies were trapped in the column due to their affinity for protein A, while the Fab224 fragments were collected in the flowthrough fraction.

Production and purification of anti-HEV Fab4. Fab4 was prepared by phage display and purified according to the protocol described previously (25). Briefly, chimpanzee 1441 was infected with HEV strain SAR-55. Bone marrow was aspirated from the iliac crest of this animal, and the antibody κ-chain gene and γ1-chain gene were amplified and cloned into the pComb3H phage display vector and pGEM-T cloning vector (Promega), respectively, and transformed into *Escherichia coli* XL-1 Blue. The bacteria were then amplified and infected with helper phage VCS M13 at a multiplicity of infection of 50 to produce a library displayed on the surfaces of phage particles. Phage was panned on SAR-55 ORF2-coated ELISA wells; four rounds of panning were performed. After amplification of the selected library, the phagemid DNA was extracted and the vector was modified to remove the bacteriophage coat protein III-encoding region of the phage. The phagemid DNAs were religated and transformed into *E. coli* XL-1 Blue to produce soluble Fabs. The vector pComb3H was constructed to encode a six-histidine tail at the end of the Fab fragment, thus facilitating Fab purification. Fab4 purity was determined by SDS-PAGE, followed by colloidal Coomassie brilliant blue staining.

Production and purification of HEV VLPs. The production and purification of HEV VLPs were conducted as described previously (13, 15, 20, 30). Briefly, DNA fragments encoding the N-truncated ORF2 protein (for the wild-type VLP) and the chimeric ORF2 protein (for VLP-C-tag) were cloned using the baculovirus transfer vector pVL1393 to yield pVLORF2. Insect Sf9 cells (Riken Cell Bank, Tsukuba, Japan) were used to produce recombinant baculovirus. Tn5 insect cells were infected with the recombinant baculoviruses at a multiplicity of infection of 5 and incubated in Ex-Cell 405 medium (JRH Biosciences, Lenexa, KS) for 6 days at 26.5°C. The supernatant was collected after the removal of cell debris by centrifugation at 10,000 × g for 90 min. The HEV VLPs were pelleted at 100,000 × g for 2 h in a Beckman SW32 Ti rotor and resuspended in 4.5 ml Ex-Cell 405. The VLPs were further purified by centrifugation through a CsCl density gradient (1.31 g/ml) at 110,000 × g for 24 h at 4°C in a Beckman SW 55 Ti rotor. The white virus band was collected and diluted 4 times with Ex-Cell 405 to decrease the CsCl concentration, and then the VLPs were centrifuged for 2 h in a Beckman TLA 55 rotor at 100,000 × g. The VLPs were resuspended in 100 to 500 µl of 10 mM potassium-MES (morpholineethanesulfonic acid) buffer (pH = 6.2) and stored at 4°C. To construct chimeric VLP-C-tag, recombinant baculoviruses were prepared by inserting the B-cell tag epitope from herpes simplex virus glycoprotein D (QPELAPEDPED) at amino acid position 608 (20).

Western blotting. A series of DNA fragments were constructed to encode truncated ORF2 residues 112 to 660, 112 to 608, 112 to 602, 112 to 601, 112 to 600, 112 to 596, and 112 to 589. These recombinant ORF2 genes were inserted into a baculovirus vector and expressed in insect cells using the protocol for VLP production, except that the recombinant proteins were recovered from the cytoplasm after lysis of the cell. Recombinant proteins were heated in 4× Laemmli sample buffer and electrophoresed under reducing conditions in a 10% SDS-polyacrylamide gel. After transfer of proteins to a polyvinylidene difluoride (PVDF) membrane, the membrane was blocked with TBS buffer (20 mM Tris, pH 7.6, NaCl) containing 0.5% Tween 20 (vol/vol) prior to overnight incubation with Fab224 fragments at a 1:10 dilution. After extensive washing with TBS buffer containing 0.05% Tween 20 (vol/vol), alkaline phosphatase-conjugated anti-mouse IgG (Fab specific) was incubated with the membrane for 1 h at room temperature. The blot was then washed and developed with the p-nitroblue tetrazolium-5-bromo-4-chloro-3-indolylphosphate (NBT-BCIP) reaction.

Preparation of VLP-Fab complexes for cryoelectron microscopy. The VLP-Fab complexes were prepared by incubating Fabs with VLPs at a molar ratio exceeding 1:300 (VLP versus Fabs) at 4°C overnight. To reduce the background density in the subsequent structural determination, highly pure VLP-Fab complexes were obtained using a short column containing Sephacryl 300, which resulted in the removal of the unbound Fab from the sample. The fractions containing VLP-Fab complexes were collected based on their optical density readings at a wavelength of 280 nm. The Fab binding occupancy was roughly estimated by performing SDS-PAGE (8-to-25% gradient) on the purified VLP-Fab complexes at a constant voltage using the Phast system (Pharmacia). The

particle morphology of VLP-Fab complexes was examined by negative-stain electron microscopy using 2% uranyl acetate.

Cryoelectron microscopy. Sample preparation and cryo-EM were performed following previously described, well-established procedures (13, 30). Briefly, a drop containing 3.5 μ l of the sample was applied to a glow-discharged holey carbon-coated copper grid, blotted with a piece of filter paper for 3 s to remove the extra liquid, and quickly plunged into liquid ethane cooled by liquid nitrogen. Samples were frozen in a thin layer of vitrified ice. The grid was then transferred into a Gatan 626DH cryo holder and kept at a low temperature (-178°C) during the subsequent data collection. Micrographs were collected under low-dose conditions ($<10\ e^{-}/\text{\AA}^2$) using Kodak SO163 film at a magnification of $\times 45,000$ on an FEI CM-120 electron microscope operated at 120 kV, and particles were photographed at a defocus range of 1,000 to 3,000 nm. Micrographs were visually inspected and selected based on a suitable particle concentration, optimal ice thickness, and minimal specimen drift. Only micrographs fulfilling these criteria were analyzed.

Image processing. Selected micrographs were digitized using a Heidelberg Primescan D8200 (Heidelberg, Germany) at a 14- μ m scanning step size, corresponding to 3.11 \AA per pixel of specimen space. Particles were manually picked and centered by cross-correlating each one against the circular average image. The astigmatism and defocus value were evaluated by the superimposed power spectra from all particles within a single micrograph. The contrast transfer function's first zero was approximately within the range of 17 to 20 \AA^{-1} for the data used for the structural determination. The self-common-lines algorithm (4) was used to yield the initial models for VLP-C-tag, VLP-Fab4, and VLP-Fab224. The origin and orientation search for each particle was carried out iteratively using the polar Fourier transformation (PFT) algorithm running on an AMD MP1800 MHz dual-processor Linux workstation (2). Three-dimensional reconstructions were computed by combining a set of particles with orientations that spread evenly in an icosahedral asymmetric unit using the Fourier-Bessel algorithm and by superimposing 5-3-2 icosahedral symmetry. To examine the reliability of the three-dimensional reconstruction, the data set was evenly divided into two parts at the final refinement step and two three-dimensional reconstructions were computed. The resolution was estimated using Fourier shell correlation (FSC) by assessing the agreement between these two reconstructions in Fourier space. Using a coefficient value of 0.5 as the criteria, the estimated resolutions of the three-dimensional reconstructions of VLP-C-tag, VLP-Fab224, and VLP-Fab4 were computed as 17.5 \AA , 18.5 \AA , and 24 \AA , respectively.

The three-dimensional reconstructions were rendered and visualized using the Chimera program (22). The contour level was chosen at a value corresponding to 100% of the mass of the PORF2 protein. The electron density map was displayed in the isosurface mode, which builds a barrier to contour the density about a certain threshold.

Fitting the crystal structure into cryo-EM density maps. The density of the bound Fab molecule was determined from a difference density map, which was calculated by subtracting the cryo-EM map of unbound HEV T=1 VLP from the density map of the Fab-VLP complex. The cryo-EM map of unbound HEV VLP was published previously (30). Because the cryo-EM data for unbound VLP and the Fab-VLP complex were collected with the same FEI CM-120 electron microscope under similar imaging conditions, the difference density map was calculated by direct subtraction of the density of unbound VLP from the reconstruction of the Fab-VLP complex after normalizing the contrast between the two maps. The calculated difference map was used as a constraint in model fitting. Manual fitting was carried out by translational and rotational movement of the three-dimensional crystal structure of the PORF2 protein (PDB ID 2ZZQ) (31) into the cryo-EM density maps using program O (9). To obtain the best fit, the atomic model of the PORF2 subunit was treated as a rigid body. The fitting was first manually refined by minimizing the clashes between symmetry-related PORF2 molecules and then evaluated based on the cross correlation coefficient (CC value) between the cryo-EM density and the density computed from the fitted PORF2 coordinates. Fitting was halted when the CC value reached 80%. The figures were prepared using the program PyMOL (5), and the surface stereographic projection of the HEV VLP was prepared using the program RIVEM (29).

RESULTS

Binding of antibody Mab224 to PORF2. The binding of the monoclonal antibody Fab224 to PORF2 was examined via immunoblot analysis. A series of recombinant ORF2 proteins with C-terminal truncations were separated by SDS-PAGE on

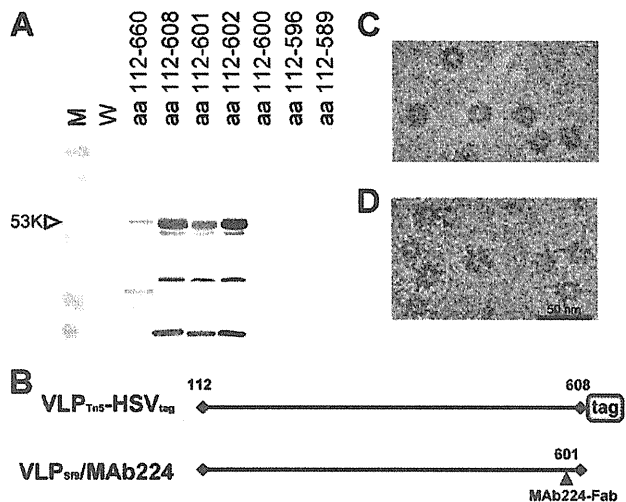


FIG. 1. Characterization of VLP-C-tag and VLP-Fab224. (A) Western blot assay of the C-terminally truncated ORF2 proteins with Fab224. M, molecular weight markers; W, peptides recovered from baculovirus-infected cells. (B) Diagram of the C-terminal markers. (C) Electron micrograph of frozen-hydrated VLP-C-tag. (D) Electron micrograph of frozen-hydrated VLP-Fab224. Black arrowheads indicate the Fab molecules attached to the VLP. Both particles showed an absence of density in the center. Note that the surface spikes in VLP-Fab224 appeared as longer thorn-like densities compared to those of VLP-C-tag.

a 10% gel under reducing conditions and blotted with Fab224 (Fig. 1A). Fab224 recognized both reduced and denatured recombinant ORF2 proteins that contained amino acids 112 to 660, 112 to 608, 112 to 602, and 112 to 601. In contrast, recombinant ORF2 proteins composed of residues 112 to 600, 112 to 596, and 112 to 589 did not bind to Fab224. These data indicate that residues 597 to 601 are critical for Fab224 binding to PORF2. Because the recombinant ORF2 proteins were recovered from cell cytoplasm where multiple forms of PORF2 were reported (15), the positive bands observed at a low molecular weight may be the proteolytic products or degraded forms of ORF2 that contain the Fab224 binding sequence.

Two-dimensional electron cryomicrographs. The chimeric VLPs (Fig. 1C) and the Fab224-conjugated VLP complex (Fig. 1D) showed circular profiles with spike-like densities that extended from the surface. As we observed previously (15, 30), they appeared to have a white, contrasting center, indicating that they are empty particles lacking RNA (data not shown). The sizes of both VLPs were approximately 27 nm without taking into account the extra densities that extended from the VLP-Fab224 surface (Fig. 1D).

Binding site of antibodies. The cryo-EM structure of HEV-Fab224 was reconstructed from 615 images of individual particles and displayed T=1 icosahedral symmetry with 60 protein subunits that were arranged into 30 dimeric protruding spikes located at each icosahedral 2-fold axis (Fig. 2A). Sixty Fab molecules were observed around each VLP particle, bound to the shoulder of the P domain. The Fab density extended $\sim 57\ \text{\AA}$ radially away from the spike surface. The density corresponding to the Fab was approximately equal in magnitude to that of the HEV VLP, indicating that most or all of the 60

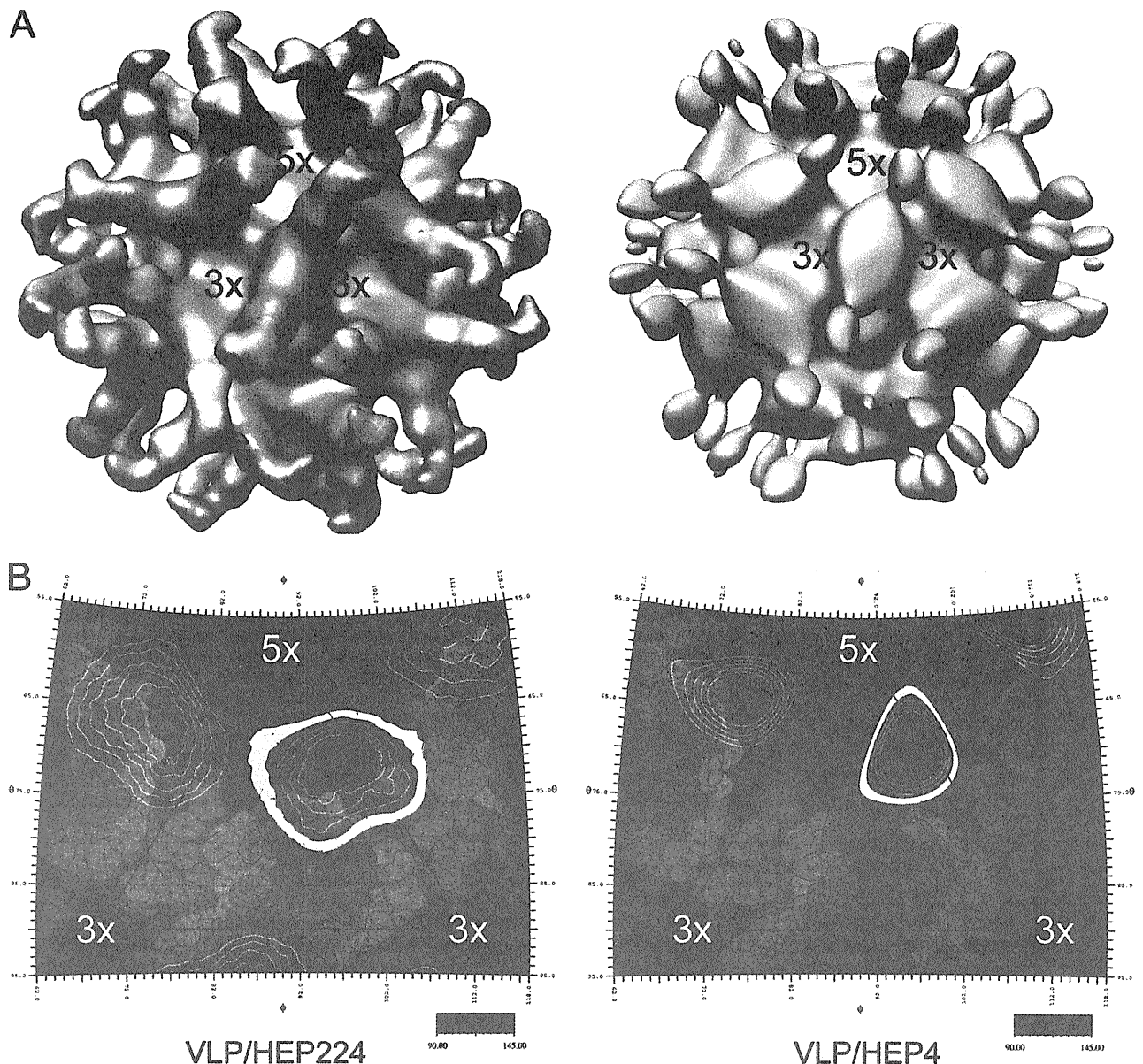


FIG. 2. The cryo-EM structure of HEV T=1 VLP in complex with anti-HEV antibodies. (A) Surface presentation of VLP-Fab224 (left) and VLP-Fab4 (right) viewed along one of the icosahedral 2-fold axes. One 5-fold axis and two adjacent 3-fold axes are marked with the corresponding number. In both reconstructions, 60 copies of Fab are attached to the lateral side of HEV VLP; however, the density of Fab4 molecules appears to be less than that of Fab224 molecules. (B) The viral surface is shown as a stereographic projection overlapped with a line drawing of an icosahedral asymmetric unit. The 5-fold and two adjacent 3-fold axes are marked with corresponding numbers, while the black triangle encloses the area of an icosahedral asymmetric unit. The surface residues are colored according to the distance from the center of the VLP, with red being the furthest away and blue representing the surface depressions. The Fab density is projected as white contour lines on the viral surface, and the outermost layer of density is drawn as thick white contour lines.

binding sites were occupied by a Fab molecule. The density corresponding to the VLP capsid was removed from the cryo-EM map, producing a Fab differential density map that was used to pinpoint the binding site of the Fab224 antibody (Fig. 3A and B).

In addition, the structure of HEV VLP in complex with the neutralizing antibody Fab4 was determined by combining 264 individual images. Fab4 precipitates both the native HEV

virion and recombinant PORF2 peptides, but the reaction depends on the presence of amino acids 597 to 607 (26). Three-dimensional reconstruction of the VLP-Fab4 complex showed 60 Fab molecules bound to each HEV VLP. Unlike the VLP-Fab224 complex, the density corresponding to Fab4 was about one-third of that of the capsid (Fig. 2A), suggesting that only 30 to 40% of the binding sites were occupied by the Fab. Moreover, the binding of Fab4 appeared to be deeper on the

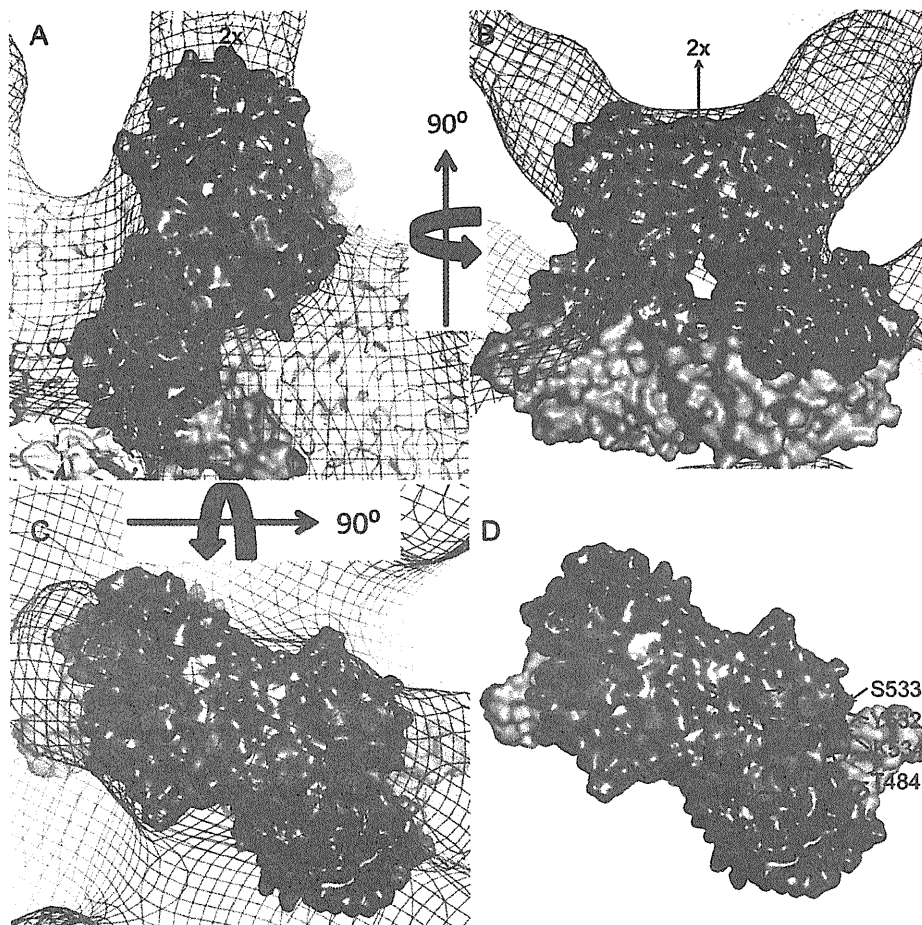


FIG. 3. The binding site of Fab224 antibody. (A) The cryo-EM density map of VLP-Fab224 was fitted with the crystal structure of PORF2 and viewed along a bound Fab molecule. One PORF2 dimer is presented as a solid surface and colored light magenta for the S domain, blue violet for the M domain, and dark gray for the P domain. The neighboring dimers are drawn in ribbon mode and colored wheat. (B) Side view of a PORF2 dimer fitted into the cryo-EM density map. (C) A PORF2 dimer viewed along the 2-fold axis and overlapped with the cryo-EM density map. (D) Top view of a PORF2 dimer viewed along the 2-fold axis. The amino acids in PORF2 responsible for binding to Fab224 are labeled. The PORF2 dimer is presented as a solid surface and colored in gray, violet, and light magenta for the P domain, the M domain, and the S domain, respectively. The residues along the Fab binding interface are colored according to the element, with green for carbon, blue for nitrogen, and red for oxygen.

side wall of the protruding domain toward the capsid shell, leaving its Fc domain exposed above the surface of the plateau (Fig. 2A). In contrast, the entire Fab224 molecule stood mainly on the top of the P domain surface. The Fab224 and the Fab4 molecules extend along the long axis of the P domain. In both cases, no steric hindrance of the Fab on the P domain with the neighboring Fab molecules at either the 5-fold or the 3-fold axes was apparent. The orientation of the Fabs relative to the plateau appeared different at a radius of 135 Å. The long axis of Fab224 tilted toward the neighboring spike, while the long axis of Fab4 pointed to the 5-fold axis (Fig. 2A).

To further analyze the Fab and HEV VLP binding interface, the crystal structure of genotype 1 PORF2 was docked onto the VLP-Fab224 cryo-EM density map. The genotype 1 PORF2 crystal structure (PDB ID 2ZZQ) is composed of three domains (31), and these domains are in good agreement with those of genotype 3 and genotype 4 PORF2 (PDB ID 2ZTN and 3HAG, respectively) (8, 32). The coordinates fitted very

well with the cryo-EM density map without any adjustment (CC value of 80%). The atoms on the surface of the HEV VLP capsid were plotted and colored according to their radial distance and overlapped with the density of the Fab at the surface plateau of the protruding spike (Fig. 2B).

The Fab224 interacted with the residues on the side of the ORF2 spike rather than with those residues on the spike's plateau surface (Fig. 3C). The contact footprint did not overlap with the dimeric interface of the PORF2 spike. As expected, Fab224 recognizes a conformational epitope, and its binding site covers a surface composed of three loops, including amino acids 470 to 493 in AB loop, amino acids 539 to 569 in CD loop, and amino acids 581 to 595 in EF loop (Fig. 3D). Residues E479, D481, T484, Y485, and S487 from the AB loop and residues Y532, S533, and K534 from the CD loop were in close contact with the Fab molecule.

Structure of HEV chimeric VLP. Chimeric HEV VLP-C-tag was constructed using a PORF2 fusion protein in which a

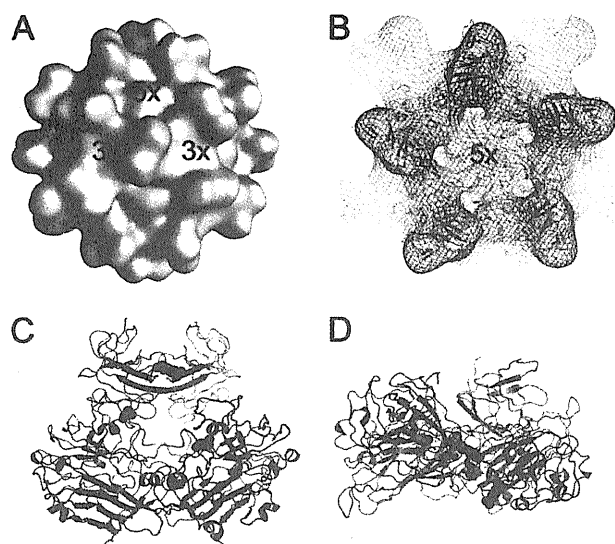


FIG. 4. The structure of the chimeric HEV VLP carrying a B-cell tag. (A) Surface presentation of VLP-C-tag viewed along an icosahedral 2-fold axis. (B) The cryo-EM density map of VLP-C-tag (mesh) was fitted with the crystal structure of the PORF2 decamer (ribbon). (C) Ribbon representation of PORF2 dimer with one monomer colored gray and the other colored pink for the S1 domain, blue for the M domain, and lime for the P domain. The amino acids prior to the four internal insertion sites are marked in sphere mode with color coding representing the elements as described in the Fig. 3 legend. (D) The top view of the PORF2 dimer, showing the location of the non-VLP insertion sites.

B-cell tag of 11 amino acids was incorporated into the C terminus of PORF2 (Fig. 1B). A total of 782 images of individual particles were used to reconstruct the final three-dimensional model of VLP-C-tag. In agreement with the previously published cryo-EM VLP structures, the surface of VLP-C-tag can

be divided into two distinct layers, an icosahedral shell and a protruding spike (Fig. 4A). The spike projects outward from the icosahedral shell and is composed of a PORF2 dimer. The distance between two adjacent spikes was ~ 76 Å as measured between the centers of the surface plateaus. These results are consistent with the measurements of VLPs obtained either from Tn5 insect cells (30) or from Sf9 insect cells (13), and no detectable density was added onto the outer surface of the spike. No RNA density was detected within the chimeric VLP-C-tag.

The crystal structure fit very well within the VLP-C-tag density map (Fig. 4B), indicating that the insertion of the C-terminal 11 amino acids inhibits neither the dimer-dimer interactions nor the formation of T=1 VLP. When the density maps were contoured to cover 100%, the radii of the S domains were roughly the same for both the VLP-C-tag and the VLP-Fab224 map, and the heights of the protruding spikes appeared similar. No density difference was observed from the docking (Fig. 5), suggesting that the inserted B-cell tag is flexible and less ordered. However, model fitting revealed that coordinates with unoccupied density appeared at the lateral side of the spike and underneath the Fab224 binding site (Fig. 5A and B), which may correspond to the inserted peptide.

DISCUSSION

HEV T=1 VLP is a vaccine candidate that induces protective immunity in nonhuman primates (12). It can also be used as an antigen carrier to deliver foreign epitopes through oral administration (20). Therefore, structural analysis of the antibody recognition sites is essential to suppress the neutralization effect of host vector-specific antibodies. For this purpose, we determined the structure of HEV VLP in complex with antibodies Fab224 (VLP-Fab224) and Fab4 (VLP-Fab4) and the structure of chimeric HEV VLP carrying a B-cell tag at the C terminus of PORF2 (VLP-C-tag). Docking the PORF2 crys-

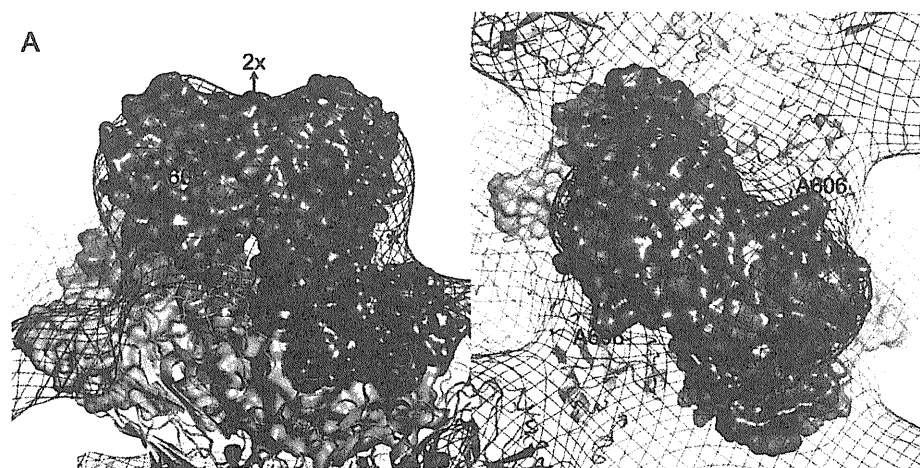


FIG. 5. Fitting of the PORF2 structure into the cryo-EM density map of HEV VLP-C-tag. The side view (A) and the top view (B) of the fitted PORF2 dimer (surface presentation) are overlapped with the cryo-EM density map of VLP-C-tag (mesh). The C-terminal residue A606 is located at the side of the protruding spike. One PORF2 dimer in the surface presentation is colored light magenta, blue violet, and gray for the S, M, and P domain, respectively. The ribbon representation shows the adjacent dimers. The amino acids in PORF2 responsible for binding to Fab224 are colored green for carbon, blue for nitrogen, and red for oxygen. Asterisks mark the location of the extra density that was not occupied with PORF2 coordinates.

tal structure provides spatial information on the HEV antigenic domain and structural guidance to better design foreign epitope insertion.

Structure of the neutralization epitopes. The antigenic properties of HEV and the mechanisms by which it is neutralized are difficult to characterize due to the lack of adequate cell culture replication systems. Therefore, our understanding of HEV immunology is mainly based on studies using recombinant proteins expressed in *E. coli* (23) and recombinant proteins or HEV VLPs generated using the baculovirus expression systems (15, 24). Data from these studies indicate that the C-terminal region of PORF2 participates in the immune response against HEV and that the HEV neutralization epitope is conformational. The minimum peptide required to induce HEV-neutralizing antibodies corresponds to a region of 148 residues in PORF2, from amino acids 459 to 607 (33). This peptide coincides with the P domain revealed in the crystal structures of PORF2. The density of the Fab in our cryo-EM structure interfaced entirely with the spikes, thus confirming that the P domain is primarily responsible for HEV antigenicity. Fab4 is a chimpanzee antibody that recognizes the ORF2 protein and was isolated from a cDNA library by using phage display (25). Fab4 binds to native HEV virions and recombinant PORF2 peptides containing amino acids 597 to 607 (26). We performed fitting with the VLP-Fab4 structure; however, the Fab4 density was too weak to conclusively determine the Fab4 binding site on the surface of HEV VLP. However, the density corresponding to the Fab4 molecule did cover amino acid 606 (data not shown). It is not clear why Fab224 appeared not to interact with peptides lacking amino acids 599 to 608 in immunoblot analysis. However, the Fab224 binding site is consistent with the critical antigenic residues determined previously using mutagenesis. It was found that double mutations that changed residues E479 and K534 or Y485 and I529 to alanine selectively abrogated PORF2's reactivity with neutralizing antibodies (11). Experiments with another set of mutants defined the same region as the HEV antigenic domain, with antibody recognition residues spreading over the AB, CD, and EF loops (32). The antibodies used in both experiments were neutralizing antibodies; therefore, the Fab224 binding surface is part of the dominant neutralization site, suggesting that the monoclonal antibody Fab224 is a neutralizing antibody. This neutralization site partially overlaps with the receptor binding site (32), and antibody binding may create spatial hindrance that prevents HEV VLPs from attaching to the cell surface.

Insertion sites for foreign epitopes. Because they are highly organized capsids that mimic the overall structure of virus particles, VLPs are a robust means by which to simultaneously carry small molecules, peptide antigenic epitopes, and DNA vaccines from heterogeneous sources to target disease sites. However, this rational vaccine design relies on excellent VLP structural information so that epitopes can be effectively conjugated to the VLP surface. In a previous study, rather than selecting PORF2 insertion sites on the basis of structural information, six insertion sites were selected according to restriction enzyme sites located either internally (four sites) or in the N or C terminus of PORF2. The internal sites are located after residues A179, R366, A507, and R542. Fusion proteins carrying insertions at sites A179 and R336 completely failed to produce VLPs, and insertions at A507 and R542 greatly re-

duced VLP production (20). Crystal structure data revealed that the spatial position of these sites is disadvantageous. Residue A179 is located in the S domain in the middle of an α -helix, which is necessary for the integrity of the S domain and its interaction with the 2-fold-related neighboring subunit. R366 is located in the M domain and favors electrostatic interaction with residue E386 from the 3-fold-related neighboring subunit. Although located within the P domain, the side chain of R542 is within the dimeric interface and guides the hydrophobic interaction of the two monomers. Replacement of R542 may misalign the orientation between two P domains and weaken the dimeric interaction between PORF2 proteins. Residue A507 in the P domain plays an important role in maintaining P domain orientation by fixing the angle of the long proline-rich hinge. Moreover, none of the four residues are exposed on the surface of VLPs, although some of them are located on the surface of individual PORF2 subunits (Fig. 4C and D). Therefore, the insertion of a foreign sequence at these sites does not interfere with the expression of individual proteins but, rather, hinders the assembly of HEV VLPs. The crystal structure revealed that the C terminus is exposed on the surface of VLPs, while the N terminus points toward the VLP center. Therefore, insertion at these two sites does not inhibit VLP assembly; however, the C terminus is more suitable for tethering bulky foreign antigenic sequences, as was shown in a previous report (20).

The cryo-EM structure of the chimeric HEV VLP-C-tag suggested that the B-cell tag was located at the lateral side of the spike, not far from residue A606 (C-terminal end in the crystal structure) (Fig. 5A). This density is located beneath the Fab224 binding site but nonetheless overlaps with the potential binding site of Fab4. As a result, the insertion of the 11-amino-acid B-cell sequence may leave the HEV antigenic site partially open and accessible to the host immune system. This explains why mice can develop antibodies against both HEV and the foreign epitope after oral administration of VLP-C-tag (20).

In conclusion, the cryo-EM structures of VLP-Fab224 identified the lateral surface of the P domain as the recognition site for anti-HEV neutralizing antibodies. The insertion of a B-cell epitope at the PORF2 C terminus does not interfere with T=1 VLP assembly. Thus, T=1 HEV VLPs are a novel tool for oral vaccine delivery, as they constitute nonreplicating entities that can induce mucosal immunity without adjuvant. The induction of antibodies against both HEV and the target disease is an additional advantage of this delivery system.

ACKNOWLEDGMENTS

We thank K. Kato for assistance with antibody preparation and N. Miyazaki for initial model fitting of the P domain structural density.

This project was supported in part by grants from the STINT Foundation, the Medical Research Council, and the PIOMS Institutional Program to R.H.C. This study was also partly funded by a grant from the Swedish Research Council to L.X. J.C.W. and L.X. were supported by grants from the Cancer Research and Discovery Programs, respectively. J.C.W. was initially supported by a grant from NSC as an exchange student under the cosupervision of D. M. Liou and Y. J. Sung.

REFERENCES

1. Adler, B., and S. Faine. 1983. A pomona serogroup-specific, agglutinating antigen in *Leptospira*, identified by monoclonal antibodies. *Pathology* 15: 247-250.